

# A Clifford Algebraic Approach to $E(n)$ -Equivariant High-order Graph Neural Networks

Hoang-Viet Tran<sup>1,\*</sup>, Thieu N. Vo<sup>1,\*</sup>, Tho Tran Huu<sup>1</sup>, Tan Minh Nguyen<sup>1</sup>

---

## Abstract

Designing neural network architectures that can handle data symmetry is crucial. This is especially important for geometric graphs whose properties are equivariance under Euclidean transformations. Current equivariant graph neural networks (EGNNs), particularly those using message passing, have a limitation in expressive power. Recent high-order graph neural networks can overcome this limitation, yet they lack equivariance properties, representing a notable drawback in certain applications in chemistry and physical sciences. In this paper, we introduce the Clifford Group Equivariant Graph Neural Networks (CG-EGNNs), a novel EGNN that enhances high-order message passing by integrating high-order local structures in the context of Clifford algebras. As a key benefit of using Clifford algebras, CG-EGNN can learn functions that capture equivariance from positional features. By adopting the high-order message passing mechanism, CG-EGNN gains richer information from neighbors, thus improving model performance. Furthermore, we establish the universality property of the  $k$ -hop message passing framework, showcasing greater expressive power of CG-EGNNs with additional  $k$ -hop message passing mechanism. We empirically validate that CG-EGNNs outperform previous methods on various benchmarks including n-body, CMU motion capture, and MD17, highlighting their effectiveness in geometric deep learning.

---

## 1. Introduction

Developing neural network architectures capable of accommodating the symmetry constraints inherent in data and transformations is essential in geometric deep learning and remains a highly active research domain [56, 38, 5]. This is especially important for graph-based applications, such as those in chemistry [42, 7, 53] and physical sciences [6, 4, 11, 54], where nodes in the graph represent points in Euclidean space and the properties of the graph stay equivariant under Euclidean transformations. Convolutional Neural Networks (CNNs), which exhibit translation equivariance, and Graph Neural Networks (GNNs),

---

\*Equal contributions.

<sup>1</sup>National University of Singapore

which demonstrate permutation equivariance, are notable examples of the significant success and effectiveness of integrating symmetry-aware structure into neural network architectures [15, 20, 41].

The  $E(n)$ -equivariant Graph Neural Network (EGNN) model, as proposed by [58], is specifically designed for graph data and can be considered as a scalarization approach. EGNN finds broader applications in drug design, molecular modeling, and 3D point cloud primarily due to its efficiency and straightforward model design [12, 43, 59]. In principle, EGNN adopts the message passing framework from GNNs and additionally incorporates the information of the distances of nodes into the message update in such a way that the equivariant property is achieved [67, 22].

Despite their effectiveness, EGNNs have limited expressive power due to its inability to distinguish individual nodes. To tackle this challenge, researchers have introduced several high-order GNNs. These models leverage an encoding of  $k$ -tuples of nodes, subgraphs, or hyper-graph and then apply either message passing techniques [52] or equivariant tensor operations [49]. High-order GNNs hold the promise of incorporating richer information from local subgraphs into the message passing process, thereby achieving superior results compared to traditional GNNs. Nevertheless, it is worth noting that despite their enhanced capabilities, these high-order GNNs lack equivariance with respect to Euclidean transformations. This absence of equivariance poses a significant drawback in specific applications within the fields of drug design, chemistry and physical sciences.

**Contributions.** In this paper, we introduce a novel class of equivariant graph neural network, named the *Clifford Group Equivariant Graph Neural Networks* (CG-EGNNs). Similar to EGNNs, our approach is based on the message passing mechanism. However, in contrast to EGNNs, *CG-EGNNs enhance the message passing process by integrating high-order local structures around graph nodes within the framework of Clifford algebras*. In addition, we prove that the  $k$ -hop message passing mechanism satisfies the universality property for geometric graphs. Therefore, CG-EGNNs with the additional  $k$ -hop message mechanism have an ability of gathering richer information from neighboring nodes during each feature update, thereby enhancing the expressive power of the networks while preserving equivariant properties. Furthermore, in our formulation, positional features are updated only once at the final layer, eliminating the need for updating positional features at every layer and consequently reducing computational complexity. Our contribution is three-fold.

1. We introduce a novel class of equivariant high-order graph neural networks, namely CG-EGNNs, which enables equivariance properties of high-order message passing process by integrating high-order local structures around graph nodes within the framework of Clifford algebras.
2. We theoretically prove that CG-EGNN is  $E(n)$ -equivariant and capable of learning functions that capture equivariance from positional features at the same time.

3. By adapting the high-order message passing mechanism, CG-EGNN can gain richer information from neighbors to each node feature updates, resulting in performance improvements. In addition, we establish the universality property of the  $k$ -hop message passing framework, indicating that CG-EGNN with  $k$ -hop message passing mechanism possesses greater expressive power.

We demonstrate the superiority of our model over previous approaches through significant empirical improvements on three benchmarks: n-body system, CMU motion capture dataset [17], and MD17 molecular dataset [16].

**Organization.** We structure this paper as follows: After summarizing related work in Section 2, we recall necessary definitions and constructions from Equivariant Graph Neural Networks and Clifford Group Equivariant Neural Networks in Section 3. In Section 4, we present the detailed construction of CG-EGNNs and discuss their equivariance the importance of Clifford Algebra in CG-EGNNs. In Section 5, we propose an addition component to CG-EGNNs using  $k$ -hop message passing framework. We theoretically prove the universality of the  $k$ -hop message passing framework for geometric GNNs, thus enhancing the expressive power of the obtained CG-EGNNs. In Section 6, we conduct experiments to justify the advantages of CG-EGNNs over previous methods in the literature. The paper ends with concluding remarks. Experimental details are provided in the Appendix.

## 2. Related Work

**Equivariant neural networks.** The equivariance property of neural networks has been achieved through various ways, with most falling into three distinct classes: scalarization methods, regular group representations, and irreducible representations [34]. Scalarization methods, such as those manipulating scalar features or vectors through scalar multiplication, have been employed, yet they often struggle to capture all directional information [19, 44, 21, 65]. Regular representation methods construct equivariant maps via integrals over the group under consideration [18, 45, 24, 9]. However, for infinite or continuous groups, the intractability of such integrals necessitates approximations that can compromise equivariance.

Irreducible representation methods, specifically designed for neural networks equivariant to  $SO(3)$  or  $O(3)$ , utilize Wigner-D matrices and Clebsch-Gordan coefficients within a steerable spherical harmonics basis [66, 25]. While promising, these methods face challenges in establishing an alternative base and computing Clebsch-Gordan coefficients, which are nontrivial [2]. Recent approaches that leverage noncommutative algebras like Hamiltonian quaternions, geometric, and Clifford algebras offer a fresh perspective [63, 62, 70, 13, 57]. Similar to scalarization methods, these approaches operate directly on vector bases, simplifying orthogonal transformations through algebraic multiplication. Thus, they have the potential to advance equivariant neural network design.

**Equivariant graph neural networks.** Among the most commonly used GNN architectures are Message Passing Graph Neural Networks, which iteratively propagate messages to compute graph representations [41, 29, 69]. Leveraging this framework, several rotational equivariant neural networks tailored for geometric graphs have been developed, exemplified by works such as those by [28, 60, 12]. Additionally, approaches similar to equivariant multilayer perceptrons have been proposed for specialized tasks involving molecules and protein structures, showcased in studies by [61, 27, 40, 39, 3, 7].

**High-order message GNNs.** A few high-order Graph Neural Networks (GNNs) have been proposed to enhance the expressive capabilities of traditional GNNs. [52] introduce a message passing mechanism tailored for k-tuples of nodes. In their initialization step, each k-tuple is labeled based on the isomorphism types of their induced subgraphs, ensuring distinct labels for differing subgraph structures [48]. Another category of high-order networks employs linear equivariant operations, interleaved with coordinate-wise nonlinearities, operating on order-k tensors comprising adjacency matrices and node attributes [49, 50, 48]. These GNNs exhibit expressive power comparable to k-GNNs and are adept at counting substructures within graphs. However, none of these models are explicitly designed to maintain equivariance to transformations in Euclidean spaces.

**Clifford Algebra.** A Clifford algebra is an algebra generated by a quadratic vector space modulo some relations about the square of a vector. This is a generalization of real numbers, complex numbers, and a number of hypercomplex number systems such as quaternions, octonions, exterior algebra, etc. [32, 31]. It is often called geometric algebra when the base quadratic space is over the real numbers [1]. Clifford algebra provides a powerful language for science and engineering that clearly describes the geometric symmetries of physical space and spacetime [8, 36, 68, 14, 10, 37]. It simplifies the action of orthogonal transformations on quadratic space through algebraic multiplication, and more generally, enables computational geometry without involving matrices or tensors [51, 64, 13, 46].

### 3. Preliminaries

**Equivariant Neural Networks.** Given two sets  $X, Y$  and a group  $G$  acting on them, a function  $\phi: X \rightarrow Y$  is called  $G$ -equivariant if  $\phi(g \cdot x) = g \cdot \phi(x)$  for all  $x \in X$  and  $g \in G$ . If  $G$  acts trivially on  $Y$ , then we say  $\phi$  is  $G$ -invariant.

**Message Passing Mechanism.** Given a graph  $\mathcal{G} = (\mathcal{V}, \mathcal{E})$  with  $M$  nodes  $i \in \mathcal{V}$  and edges  $e_{i,j} \in \mathcal{E}$ . Each node  $i \in \mathcal{V}$  is associated with a node feature embedding  $\mathbf{h}_i \in \mathbb{R}^{\text{nf}}$ . Message Passing Mechanism refers to sharing information between nodes in a graph along the edges. Following the notation in [30], the message passing layer can be presented as follows:

$$\mathbf{m}_{i,j} = \phi_m(\mathbf{h}_i^l, \mathbf{h}_j^l, e_{i,j}), \quad \mathbf{h}_i^{l+1} = \phi_h \left( \mathbf{h}_i^l, \sum_{j \in \mathcal{N}(i)} \mathbf{m}_{i,j} \right),$$

where  $\mathbf{h}_i^l \in \mathbb{R}^{\text{nf}}$  is the node feature embedding of node  $i$  at layer  $l$ .  $a_{ij}$  is the edge attribute. Here,  $\phi_m, \phi_h$  are learnable neural networks.

**Equivariant Graph Neural Networks.** In the original setting of EGNN [58], each nodes  $i \in \mathcal{V}$  is additionally associated with  $\mathbf{x}_i \in \mathbb{R}^n$  as an  $n$ -dimensional coordinate embedding. The main component of EGNN is the Equivariant Graph Convolution Layer (EGCL) which takes  $(\mathbf{x}^l, \mathbf{h}^l)$  as input and outputs  $(\mathbf{x}^{l+1}, \mathbf{h}^{l+1})$ , as follows:

$$\begin{aligned} \mathbf{m}_{i,j} &= \phi_m(\mathbf{h}_i^l, \mathbf{h}_j^l, \|\mathbf{x}_i^l - \mathbf{x}_j^l\|_2^2, e_{i,j}), \\ \mathbf{x}_i^{l+1} &= \mathbf{x}_i^l + \frac{1}{M-1} \sum_{j \neq i} (\mathbf{x}_i^l - \mathbf{x}_j^l) \phi_x(\mathbf{m}_{i,j}), \quad \mathbf{h}_i^{l+1} = \phi_h \left( \mathbf{h}_i^l, \sum_{j \in \mathcal{N}(i)} \mathbf{m}_{i,j} \right). \end{aligned} \quad (1)$$

In [58], it has been proved that EGCL is  $E(n)$ -equivariant, i.e.,  $Q \cdot \mathbf{x}^{l+1} + g, \mathbf{h}^{l+1} = \text{EGCL}(Q \cdot \mathbf{x}^l + g, \mathbf{h}^l)$ , for all orthogonal matrix  $Q \in O(n)$  and translation vector  $g \in \mathbb{R}^n$ .

**Clifford Algebra and Clifford Group Equivariant Neural Networks.** Let  $\mathbb{F}$  be a field with  $\text{char } \mathbb{F} \neq 2$ . Clifford Algebra [26, 57], denoted as  $\text{Cl}(V, \mathfrak{q})$  where  $(V, \mathfrak{q})$  is a quadratic space over  $\mathbb{F}$ , is the  $\mathbb{F}$ -algebra generated by generated by  $V$  with relations  $v^2 = \mathfrak{q}(v)$  for all  $v \in V$ . The authors in [57] introduced a variant of Clifford Group and provided a class of neural networks, named Clifford Group equivariant neural networks (CGENN), that operate on elements of Clifford Algebra. It is worth noting that, when  $(V, \mathfrak{q})$  is the vector space  $\mathbb{R}^n$  with quadratic form  $\mathfrak{q}$  is the square of the Euclidean norm, i.e.,  $\mathfrak{q}(\cdot) = \|\cdot\|_2^2$ , the corresponding Clifford group is closely related to the orthogonal group  $O(n)$ , defined as

$$O(n) = \{Q \in \text{GL}(n) \mid Q^\top Q = QQ^\top = I_n\}. \quad (2)$$

This relation between the Clifford group and  $O(n)$  allows us to leverage CGENNs to build  $O(n)$ -equivariant or invariant neural networks.

#### 4. Clifford Group Equivariant Graph Neural Networks

In this section, we present our CG-EGNNs by extending EGNNs in the context of Clifford algebras. We then discuss further improvements using high-order inputs.

##### 4.1. Clifford Group Equivariant Graph Neural Networks (CG-EGNNs)

Following notations from the original setting of EGNNs, we consider a graph  $\mathcal{G} = (\mathcal{V}, \mathcal{E})$  with  $M$  nodes  $i \in \mathcal{V}$  and edges  $e_{i,j} \in \mathcal{E}$ . To present the architecture of our model, let us assume that each node  $i \in \mathcal{V}$  is associated with an initial position  $\mathbf{x}_i \in \mathbb{R}^n$ , some vector features  $\mathbf{v}_i = (\mathbf{v}_{i,1}, \dots, \mathbf{v}_{i,r}) \in \mathbb{R}^{n \times r}$ , and some scalar features  $a_i = (a_{i,1}, \dots, a_{i,s}) \in \mathbb{R}^s$ . Depending on particular experiments, vector features can be either velocity or acceleration, while scalar features can be mass, charge, temperature, and so on.

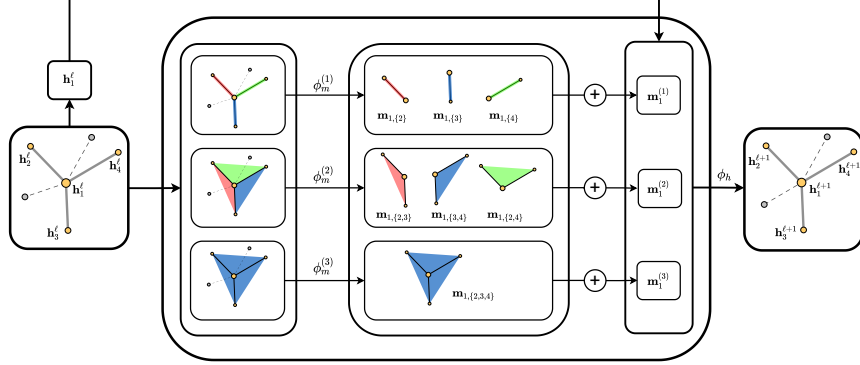


Figure 1: Illustration of high-order message passing mechanism (Eqs. (4)-(6)) in CG-EGNN. Here, the feature of node 1 is updated by computing and aggregating messages of order  $d = 1, 2, 3$  from its neighborhood  $\mathcal{N}(1) = \{2, 3, 4\}$ .

CG-EGNNs will preserve equivariance on the set of vector features and invariance on the set of scalar features to Euclidean group  $E(n)$ . It has three main components: the embedding layer, the Clifford graph convolution layer, and the projection layer.

**Embedding Layer.** This layer transforms the initial information at each node into multivector  $\mathbf{h}_i^0 \in \text{Cl}(\mathbb{R}^n)^{\text{nf}}$ , of the Clifford algebra  $\text{Cl}(\mathbb{R}^n)$ . By using the identifications  $\text{Cl}(\mathbb{R}^n)^{(0)} \equiv \mathbb{R}$  and  $\text{Cl}(\mathbb{R}^n)^{(1)} \equiv \mathbb{R}^n$ , we can view the position  $\mathbf{x}_i$  and the vector features  $\mathbf{v}_{i,j}$  as elements of order 1, and the scalar features  $a_{i,j}$  as elements of order 0 of the Clifford algebra  $\text{Cl}(\mathbb{R}^n)$ . The output  $\mathbf{h}_i^0$  of this layer is determined by:

$$\mathbf{h}_i^0 = \phi_{\text{embed}}(\mathbf{x}_i, \mathbf{v}_{i,1}, \dots, \mathbf{v}_{i,r}, a_{i,1}, \dots, a_{i,s}). \quad (3)$$

Here,  $\phi_{\text{embed}}$  is a learnable Clifford neural network.

**Clifford Graph Convolution Layer.** The Clifford graph convolution layer takes as input the multivector features  $\mathbf{h}^l = \{\mathbf{h}_i^l\}_{i \in \mathcal{V}}$  and edge information  $\mathcal{E} = \{e_{i,j}\}$ . Its outputs are the multivector features  $\mathbf{h}^{l+1} \in \text{Cl}(\mathbb{R}^n)^{\text{nf}}$ . In contrast to the original EGNNs, we incorporate not only messages from neighboring nodes but also messages from higher-dimensional neighbor structures into the update of multivector features  $\mathbf{h}^{l+1}$ . In particular, fix a positive integer  $D$  representing the highest-order of the neighbor structures that we want to incorporate. For each  $d = 1, \dots, D$ , and each subset  $A \subseteq \mathcal{N}(i)$  with  $d$  elements, we determine the message from  $A$  contributing to the node  $i$  as follows:

$$\mathbf{m}_{i,A} = \phi_m^{(d)} \left( \mathbf{h}_i^l, \sum_{j \in A} \mathbf{h}_j^l \right). \quad (4)$$

We can optionally add information about edge attributes to increase expressivity by concatenating them to the input of the function in a suitable way. Then, we

incorporate these messages to the multivector feature  $\mathbf{h}_i^{l+1}$  as follows:

$$\mathbf{m}_i^{(d)} = \sum_{A \subseteq \mathcal{N}(i), |A|=d} \mathbf{m}_{i,A}, \quad d = 1, \dots, D, \quad (5)$$

$$\mathbf{h}_i^{l+1} = \phi_h(\mathbf{h}_i^l, \mathbf{m}_i^{(1)}, \dots, \mathbf{m}_i^{(D)}). \quad (6)$$

Here,  $\phi_m^{(d)}$ 's and  $\phi_h$  are learnable Clifford neural networks. A visualization of a Clifford Graph Convolution Layer is given in Figure 1.

**Projection Layer.** The embedding layer let us embed input into a multivector  $\mathbf{h}_i^0 \in \text{Cl}(\mathbb{R}^n)^{\text{nf}}$ . We now need to extract information from the obtained multivector  $\mathbf{h}_i^L \in \text{Cl}(\mathbb{R}^n)^{\text{nf}}$  to get the output of the model. This is based on the objects to be predicted. If we want to predict the vector features, for example, the final position  $\mathbf{x}_i^L \in \text{Cl}^{(1)}(\mathbb{R}^n) \equiv \mathbb{R}^n$ , we compute it as follows:

$$\mathbf{x}_i^L = \mathbf{x}_0 + \phi_x(\mathbf{h}_i^L)^{(1)}, \quad (7)$$

where  $\cdot^{(1)}$  is the projection of  $\text{Cl}(\mathbb{R}^n)$  onto subspace  $\text{Cl}^{(1)}(\mathbb{R}^n)$ . Similarly, if we want to predict some scalar information of vertices, let say **output** $_i^L \in \text{Cl}^{(0)}(\mathbb{R}^n) \equiv \mathbb{R}$ , we use the projection  $\cdot^{(0)}$  of  $\text{Cl}(\mathbb{R}^n)$  onto subspace  $\text{Cl}^{(0)}(\mathbb{R}^n)$  and compute the result as follows:

$$\mathbf{output}_i^L = \phi_{\text{output}}(\mathbf{h}_i^L)^{(0)}. \quad (8)$$

Here,  $\phi_x$  and  $\phi_{\text{output}}$  are learnable linear Clifford layers. Note that we specifically use different projections of the Clifford algebra base on we want the model to be invariant or equivariant.

Overall, the CG-EGNN is a composition of the embedding layer,  $L$  Clifford graph convolution layers, and the projection layer.

**Remark 4.1.** *To archive  $E(n)$ -equivariance, at the embedding layer, we input the mean-subtracted positions. This maintains translation invariance. In some tasks that we want to predict position information, the residual connection in Eq. (7) maintains translation equivariance.*

#### 4.2. $E(n)$ -equivariant Property of CG-EGNNs

We consider our CG-EGNN consists of the embedding layer in Eq. (3),  $L$  Clifford graph convolution layers in Eq. (4), (5), and (6), and finally the projection layer in Eq. (7). We also center the input by taking the mean-subtracted position of  $\mathbf{x}_i$  in Eq. (3). We provide formal proofs for the below statements in Appendix Appendix D.

**Proposition 4.2.** *The following maps are  $O(n)$ -equivariant:*

1. The map in Eq. (3):

$$\begin{aligned} \mathbf{Embedding}: \text{Cl}(\mathbb{R}^n)^{1+r+s} &\longrightarrow \text{Cl}(\mathbb{R}^n)^{\text{nf}} \\ (\mathbf{x}_i, \mathbf{v}_i, a_i) &\longmapsto \mathbf{h}_i^0. \end{aligned} \quad (9)$$

2. The map in Eq. (4), Eq. (5), Eq. (6):

$$\begin{aligned} \mathbf{Convolution}: \text{Cl}(\mathbb{R}^n)^{\text{nf}} &\longrightarrow \text{Cl}(\mathbb{R}^n)^{\text{nf}} \\ \mathbf{h}_i^l &\longmapsto \mathbf{h}_i^{l+1}. \end{aligned} \quad (10)$$

3. The map in Eq. (7):

$$\begin{aligned} \mathbf{Projection}: \text{Cl}(\mathbb{R}^n)^{\text{nf}} &\longrightarrow \text{Cl}(\mathbb{R}^n) \\ \mathbf{h}_i^L &\longmapsto \phi_x(\mathbf{h}_i^L)^{(1)}. \end{aligned} \quad (11)$$

**Remark 4.3.** Note that  $\mathbf{h}_i^0$  is  $O(n)$ -equivariant to  $(\mathbf{x}_i, \mathbf{v}_i, a_i)$ ;  $\mathbf{m}_{i,A}, \mathbf{m}_i^{(d)}, \mathbf{h}_i^{l+1}$  are  $O(n)$ -equivariant to  $\mathbf{h}_i^l$ ; and  $\phi_x(\mathbf{h}^L)^{(1)}$  is  $O(n)$ -equivariant to  $\mathbf{h}_i^L$ .

**Remark 4.4.** Inductively, a composition of these above layers will also be  $O(n)$ -equivariant.

By the semidirect product  $E(n) = T(n) \rtimes O(n)$ , where  $T(n)$  is the translational group, inputting the mean-subtracted positions and composing with residual connection in Eq. (7) makes CG-EGNN achieves translation equivariance. In particular, messages  $\mathbf{m}_{i,A}, \mathbf{m}_i^{(d)}$  and features  $\mathbf{h}_i^l$  are  $T(n)$ -invariant, and position  $\mathbf{x}_i^L$  is  $T(n)$ -equivariant to initial position  $\mathbf{x}_i$ . Hence, our model becomes  $E(n)$ -equivariant. We summarize our results by the following corollary.

**Corollary 4.5.** CG-EGNN is  $E(n)$ -equivariant. Concretely, we have:

$$Q \cdot \mathbf{x}^L + g = \text{CG-EGNN}(Q \cdot \mathbf{x} + g), \quad (12)$$

for all orthogonal matrix  $Q \in O(n)$  and translation vector  $g \in \mathbb{R}^n$ .

### 4.3. Learning Functions that Capture Positional Equivariance by Clifford Algebras

As one of the key benefits of using Clifford algebra, our CG-EGNNs can learn the component that captures positional equivariance and invariance from the input. Indeed, the main component that captures equivariance in many previous equivariant graph neural network architectures [66, 44, 59, 58] is the Euclidean norm  $\|\mathbf{x}_i - \mathbf{x}_j\|_2^2$  given in Eq. (1), which is  $E(n)$ -invariant. In CG-EGNNs, instead of fixing such a component from the input, we directly embed inputs into the Clifford algebra and let the CG-EGNN maintain equivariance by learning implicit components that capture both positional invariance and equivariance by itself.

The implicit components that capture positional equivariance and invariance learned by CG-EGNNs are quite flexible since the Clifford layers presented in [57] provide a good class of learnable maps that is  $O(n)$ -equivariant and invariant. For example, all polynomials with real coefficients are  $O(n)$ -equivariant. The Euclidean norm, which is the fixed component used in the existing models, is a special case of a polynomial of degree 2 in the quadratic space  $(\mathbb{R}^n, \|\cdot\|_2^2)$  as

$$\|x\|_2^2 = \mathbf{q}(x) = (x^2)^{(0)}. \quad (13)$$



As our experiment results indicated below, CG-EGNNs outperform the existing models since they can flexibly choose to learn their suitable components.

Moreover, CG-EGNNs achieve better performance in most cases when high-order messages are involved. One advantage of our model is, with the Clifford layers, to incorporate high-order messages. We simply aggregate features of neighbors of vertex  $i$  and put it through such layers together with features of  $i$ . Compared to different works from the literature, we have to find a function for more than two position information, that can capture equivariance like the Euclidean norm. This approach is non-intuitive and impractical. More importantly, it is likely to result in the loss of information about the initial position of the system.

## 5. Adding $k$ -hop Message Passing Mechanism to CG-EGNNs

### 5.1. Necessity of Adding the $k$ -hop Message Passing to CG-EGNNs

The Clifford graph convolution layer presented in Section 4 has an ability of gaining richer information from neighbors to each node feature update. However, in some special cases that the graph has only a few edges, such as trees, this ability becomes unclear. The main reason is that, in this case, each node does not have enough neighbors to compute even one high-order message. Then, the messages  $\mathbf{m}^{(d)}$  for some  $d > 1$  will disappear. We can ignore this issue if we only compute high-order messages at nodes that have enough neighbors and leave the high-order messages at the remaining nodes to be none (which is zero, by Eq. (5)). Alternatively, we skip the adjacency matrix and assume the graph is fully connected. Both of these approaches might not scale well to large graphs because there is the risk of losing or overflowing information. To solve this issue efficiently, for each node  $i$ , we can consider the exchange of messages at  $i$  to a suitably larger set of vertices than the neighborhood of  $i$ . We will replace the neighborhood  $\mathcal{N}(i)$  of  $i$  by a larger set, which is the  $k$ -hop neighborhood for a positive integer  $k$ , defined as follows:

$$\mathcal{N}^k(i) = \{j \in \mathcal{V} \mid d_G(i, j) \leq k \text{ and } j \neq i\}. \quad (14)$$

In other words,  $\mathcal{N}^k(i)$  is the set of nodes  $j$  that differs from  $i$  such that there exists a path of length at most  $k$  from  $i$  to  $j$ . Note that  $\mathcal{N}^1(i) = \mathcal{N}(i)$ . Now, for each  $i \in \mathcal{V}$  and  $d = 1, \dots, D$ , we compute message from each subset  $A \subseteq \mathcal{N}^k(i)$  with  $d$  elements contributing to the node  $i$  as in Eq. (4):

$$\mathbf{m}_{i,A} = \phi_m^{(d)} \left( \mathbf{h}_i^l, \sum_{j \in A} \mathbf{h}_j^l \right), \forall A \subseteq \mathcal{N}^k(i), |A| = d, \quad (15)$$

and rewrite Eq. (5) as:

$$\mathbf{m}_i^{(d)} = \sum_{A \subseteq \mathcal{N}^k(i), |A|=d} \mathbf{m}_{i,A}, \quad d = 1, \dots, D. \quad (16)$$

In our experiments, graphs considered in the n-body system are complete graphs, but the ones in CMU Motion Capture and MD17 are trees or trees with a few additional edges. So using the  $k$ -hop neighborhood in these cases will be reasonable and necessary.

### 5.2. Universality of the $k$ -hop message passing mechanism in geometric GNNs

To verify the universality of  $k$ -hop message passing mechanism of geometric GNNs, let us forget the Clifford algebraic structure and the high-order component for a while, and consider node features of the geometric graphs as vectors in  $\mathbb{R}^d$  as in the original setting.

The universality or the expressive power of the  $k$ -hop message passing GNNs for generic graphs has been intensively studied in the literature (see for instance in [23]). However, unlike generic graphs, a geometric graph is a special kind of graph whose nodes are associated with coordinate features in  $\mathbb{R}^d$ . Because of the node features, two geometric graphs having the same combinatorial graph structure can be different in the geometric sense. Therefore, the results of the universality of generic graphs cannot be applied directly to those of geometric graphs. To tackle this issue, we establish the universality of the  $k$ -hop message passing mechanism for geometric GNNs.

Let us consider a graph  $G$  with  $M$  nodes which are points in  $\mathbb{R}^d$ . By using normalization if necessary, we can assume that  $G$  is a subset of the box  $[0, 1]^d \subset \mathbb{R}^d$ . According to the limitation of handling small numbers by computers, we can assume that the distance of every two distinct nodes of a considered graph is always greater than a fixed small real number  $\alpha > 0$ . Let  $\mathcal{X}$  be the space of all such graphs defined as

$$\mathcal{X} = \{G \subset [0, 1]^d \text{ with } |G| = M \mid \text{for all } x \neq y \text{ in } G : \|x - y\|_\infty \geq \alpha\}. \quad (17)$$

A graph neural network can now be simply regarded as a parametrized function that maps each graph in  $\mathcal{X}$  to a prediction vector in  $\mathbb{R}^r$ . In this section, we will prove that our models constructed according to the design in Section 4, but without the context of Clifford algebras, can be used to approximate any continuous function from  $\mathcal{X}$  to  $\mathbb{R}^r$ .

For each pair of graphs  $G, G'$  in  $\mathcal{X}$ , the Hausdorff distance  $d_H$  between  $G$  and  $G'$  is defined as

$$d_H(G, G') = \max\left\{\sup_{z \in G} \inf_{z' \in G'} \|z - z'\|_\infty, \sup_{z' \in G'} \inf_{z \in G} \|z - z'\|_\infty\right\}. \quad (18)$$

Given this distance function, the space  $\mathcal{X}$  becomes a compact metric space [35]. Therefore, we can discuss continuous functions on  $\mathcal{X}$  with respect to this metric. The proof for the following theorem can be found in Appendix Appendix E.

**Theorem 5.1.** *Let  $f: \mathcal{X} \rightarrow \mathbb{R}^r$  be a continuous map. Then for every  $\epsilon > 0$ , there exists a positive integer  $N$ , continuous functions  $\phi_m: \mathbb{R}^d \rightarrow \mathbb{R}^N$  and  $\phi_h: \mathbb{R}^N \rightarrow \mathbb{R}^r$  such that:*

$$\left\|f(G) - \phi_h\left(\sum_{z \in G} \phi_m(z)\right)\right\|_\infty < \epsilon, \quad (19)$$

Table 1: MSE ( $\times 10^{-2}$ ) of N-body experiment. Results averaged across 4 runs.

| GNN  | TFN  | SE(3)-Tr. | Radial Field | EGNN | SEGNN | CGENN              | CG-EGNN            |                    |                    |
|------|------|-----------|--------------|------|-------|--------------------|--------------------|--------------------|--------------------|
|      |      |           |              |      |       |                    | 1                  | 1-2                | 1-2-3              |
| 1.07 | 2.44 | 2.44      | 1.04         | 0.70 | 0.43  | <u>0.39 ± 0.01</u> | <u>0.39 ± 0.01</u> | <b>0.35 ± 0.01</b> | <b>0.35 ± 0.01</b> |

Table 2: MSE ( $\times 10^{-2}$ ) of CMU motion capture with [39] settings and [33] settings. Results averaged across 4 runs.

| Model              | GNN      | TFN      | SE(3)-Tr. | Radial Field | EGNN     | GMN      | EGHN    | CG-EGNN-1         | CG-EGNN-1-2       |
|--------------------|----------|----------|-----------|--------------|----------|----------|---------|-------------------|-------------------|
| Settings from [39] | 67.3±1.1 | 66.9±2.7 | 60.9±0.9  | 197.0±1.0    | 59.1±2.1 | 43.9±1.1 | -       | <u>23.2 ± 3.3</u> | <b>18.0 ± 0.6</b> |
| Settings from [33] | 36.1±1.5 | 32.0±1.8 | 31.5±2.1  | 188.0±1.9    | 28.7±1.6 | 21.6±1.5 | 8.5±2.2 | <u>4.9 ± 0.6</u>  | <b>4.3 ± 0.3</b>  |

for every graph  $G$  in  $\mathcal{X}$ .

**Remark 5.2** (Universality). *In Theorem 5.1, the continuous function  $\phi_h(\cdot)$  stands for the aggregation  $\phi_h(\mathbf{h}_i^l, \cdot)$ , while the continuous function  $\phi_m(\cdot)$  stands for the message  $\phi_m(\mathbf{h}_i^l, \cdot)$  (see Eqs. (4)-(6) in the Clifford Graph Convolution Layer). However, to have the sum  $\sum_{z \in G} \phi_m(z)$  in the message passing process, two conditions are required: first, the graph  $G$  is connected (which is often the case), and second, the  $k$ -hop neighborhood  $\mathcal{N}^k$  must be large enough to cover all nodes of the graph. In practice, increasing  $k$  will increase the size of the  $k$ -hop neighborhood  $\mathcal{N}^k$  very fast. However, to achieve satisfactory results in experiments, there is no need to increase  $k$  too much. In addition, the functions  $\phi_h$  and  $\phi_m$  can be approximated further by MLPs regarding the universal approximation theorem [55]. As a consequence, this theorem asserts the universality of the  $k$ -hop message passing mechanism.*

**Remark 5.3.** *In Theorem 5.1, the composition  $\phi_h \circ \sum \circ \phi_m$  is equivariant with respect to the permutation group but not the orthogonal group. The Clifford group structures play the role of adding the equivariant property (with respect to the orthogonal group) but still keep the high-order message passing mechanism of the original form to maintain the universality as much as possible.*

## 6. Experimental Results

In the experiment session, we demonstrate that CG-EGNN attains top performance compared to other equivariant models across different benchmarks. For our CG-EGNN models, we denote the variant that incorporates only first-order messages as CG-EGNN-1, the variant that incorporates both first-order and second-order messages as CG-EGNN-1-2, and analogously for other combinations of message orders. The training setups are kept as similar to the other baselines as possible. All the hyperparameter settings and experiment details can be found in Appendix Appendix F.

**N-body System.** We conduct the n-body experiment to measure the performance of our model on the task of simulating physical systems. In this experiment, we simulate the dynamics of  $n = 5$  charged particles in a 3D space.

Table 3: MSE ( $\times 10^{-2}$ ) on MD17 dataset. Results averaged across 4 runs.

|             | Aspirin            | Benzene             | Ethanol            | Malonaldehyde       | Naphthalene        | Salicylic          | Toluene             | Uracil             |
|-------------|--------------------|---------------------|--------------------|---------------------|--------------------|--------------------|---------------------|--------------------|
| RF          | 10.94±0.01         | 103.72±1.29         | 4.64±0.01          | 13.93±0.03          | 0.50±0.01          | 1.23±0.01          | 10.93±0.04          | 0.64±0.01          |
| TFN         | 12.37±0.18         | 58.48±1.98          | 4.81±0.04          | 13.62±0.08          | 0.49±0.01          | 1.03±0.02          | 10.89±0.01          | 0.84±0.02          |
| SE(3)-Tr.   | 11.12±0.06         | 68.11±0.67          | 4.74±0.13          | 13.89±0.02          | 0.52±0.01          | 1.13±0.02          | 10.88±0.06          | 0.79±0.02          |
| EGNN        | 14.41±0.15         | 62.40±0.53          | 4.64±0.01          | 13.64±0.01          | 0.47±0.02          | 1.02±0.02          | 11.78±0.07          | 0.64±0.01          |
| EGNNReg     | 13.82±0.19         | 61.68±0.37          | 6.06±0.01          | 13.49±0.06          | 0.63±0.01          | 1.68±0.01          | 11.05±0.01          | 0.66±0.01          |
| GMN         | 10.14±0.03         | 48.12±0.40          | 4.83±0.01          | 13.11±0.03          | 0.40±0.01          | 0.91±0.01          | 10.22±0.08          | 0.59±0.01          |
| GMN-L       | 9.76±0.11          | 54.17±0.69          | <b>4.63 ± 0.01</b> | <b>12.82 ± 0.03</b> | 0.41±0.01          | <u>0.88 ± 0.01</u> | 10.45±0.04          | 0.59±0.01          |
| CG-EGNN-1   | <u>9.47 ± 0.09</u> | <u>38.14 ± 0.44</u> | 4.65±0.01          | <b>12.82 ± 0.03</b> | <u>0.33 ± 0.01</u> | 0.91±0.04          | <u>10.13 ± 0.04</u> | <u>0.55 ± 0.01</u> |
| CG-EGNN-1-2 | <b>9.39 ± 0.06</b> | <b>37.45 ± 0.30</b> | <u>4.64 ± 0.01</u> | <u>12.84 ± 0.05</u> | <b>0.31 ± 0.01</b> | <b>0.82 ± 0.02</b> | <b>10.11 ± 0.04</b> | <b>0.54 ± 0.01</b> |

We train our CG-EGNN networks with 4 different seeds and compare the performance with the following baselines: GNN [30], TFN [66], SE(3)-Transformer [25], Radial Field [44], EGNN [58], SEGNN [12], and CGENN [57].

The results presented in Table 1 indicate that CG-EGNN-1-2 significantly outperforms all other baselines, achieving the lowest Mean Squared Error (MSE) for this task. This illustrates that by incorporating high order messages, our CG-EGNN-1-2 and CG-EGNN-1-2-3 exhibit enhanced capabilities in modeling physical systems compared to the baselines. While incorporating third-order messages does not yield performance gains in this experiment, we argue that higher-order messages become more beneficial as the graph size increases. Since this experiment only involves graphs with 5 nodes, the advantages of higher-order messages may not have been fully realized. We demonstrate the impact of higher-order messages for other tasks with more nodes in the ablation study below.

**CMU Motion Capture.** In the first experiment, we keep all settings the same as GMN paper [39] and use the sets of sticks and hinges from [39] embedded as the edge features. Table 2 demonstrates that CG-EGNN-1 outperforms the baselines EGNN, GMN by a large margin, and adding the second-order messages, CG-EGNN-1-2 further lowers the MSE. In the second experiment, we adopt the experiment settings detailed in the EGHN paper [33]: the node feature is augmented by the  $z$ -axis coordinates, resulting in a model that is height-aware and maintains equivariance in the horizontal directions. Table 2 also demonstrates that our model persistently outperforms the baseline models under the new distinct settings. Specifically, the MSE of our model is nearly halved compared to EGHN, and only a small fraction of EGNN and GMN.

**MD17.** Table 3 demonstrated that CG-EGNN-1-2 attains the lowest MSE for 6 out of 8 molecules and our models have the lowest MSE in general. It is noteworthy that CG-EGNN-1-2 exhibits significantly better performance on more complex, cyclic molecules, namely aspirin, benzene, naphthalene, salicylic, toluene, and uracil while remaining competitive other simpler, open-chain molecules. Figure F.2 from Appendix Appendix F visualizes the clear distinction between the more complex molecules and the simpler molecules in the dataset. This observation serves as a strong indication of our model’s ability in capturing high-order information inherent in the molecular graphs.

**5D Convex Hulls.** To evaluate the performance of the CG-EGNN model on higher-dimensional data, we conduct an experiment estimating the volume of

Table 4: Prediction error of the 5D Convex Hulls experiment. Results for EMPSN and CSMPN are as reported in [46].

| Model                | GNN    | EGNN   | CGENN  | EMPSN  | CSMPN         | CG-EGNN-1 | CG-EGNN-1-2   |
|----------------------|--------|--------|--------|--------|---------------|-----------|---------------|
| MSE ( $\downarrow$ ) | 0.0317 | 0.0123 | 0.0152 | 0.0070 | <u>0.0020</u> | 0.0055    | <b>0.0009</b> |

5D convex hulls, following the methodology outlined in the work of [46]. Table 4 demonstrates that our CG-EGNN-1-2 attains the best performance, with MSE of 0.0009. Notably, the second-best model is CSMPN, which is also a higher-order message passing network. These results provide strong evidence that higher-order message passing architectures can significantly enhance performance on tasks involving higher-dimensional data.

**Ablation study on the effect of including high order messages on 3D convex hull dataset.** We perform an ablation study on the effect of each combination of high-order messages up to order 3 on the performance of our CG-EGNN models. For this task, we run 3 sub-experiments estimating the volume of a 3D convex hull with the number of nodes per graph  $\in \{6, 7, 8\}$ .

The results reported in Table F.5 empirically validate the significant performance gains achieved by the CG-EGNN model when incorporating higher-order message passing. The CG-EGNN-2 variant has the best performance among the models considering one message order. Furthermore, the CG-EGNN-1-2 model is the top-performing architecture when two message orders are included. Additionally, the CG-EGNN-1-2-3 variant, encompassing three message orders, outperforms all other models. These findings provide strong empirical evidence that including more higher order messages enables more effective learning of intricate geometric representations, thereby enhancing the model’s ability to capture complex structural patterns. Additionally, all model runtime are reported in Table F.6 from Appendix Appendix F.6. Consistent with previous research on using Clifford algebra to construct neural networks, our models exhibit higher time complexity compared to other models. Enhancing the time complexity of Clifford GNNs by optimizing the implementation of Clifford algebra operators remains an open challenge for future work.

## 7. Concluding Remarks

We introduced a novel  $E(n)$ -equivariant graph neural network that incorporates a high-order message passing mechanism within the framework of Clifford algebras. Unlike previous equivariant graph neural networks, our model has the ability to learn its favorite equivariant functions from the positional features of data points, thereby extracting more comprehensive information from neighboring nodes during the message passing process. This enhanced capability enables our model to capture equivariance effectively, while harnessing the expressive power inherent in high-order message passing mechanisms. We believe that these properties make our approach highly effective in geometric deep learning promising in various applications in the fields of chemistry and physical sciences. A limitation of our method, as well as other existing models built upon Clifford

algebras, is the increased computational cost of the high-order message passing mechanism. However, we have already made significant improvements in experiments by adjusting key components of GNNs while maintaining number of parameters, so we are optimistic about future advancements in this direction.

## References

- [1] Rafal Ablamowicz, Garret Sobczyk, et al. *Lectures on Clifford (geometric) algebras and applications*. Springer, 2004.
- [2] Arne Alex, Matthias Kalus, Alan Huckleberry, and Jan von Delft. A numerical algorithm for the explicit calculation of  $SU(N)$  and  $SL(N, C)$  Clebsch-Gordan coefficients. *Journal of Mathematical Physics*, 52(2), 2011.
- [3] Brandon Anderson, Truong Son Hy, and Risi Kondor. Cormorant: Covariant molecular neural networks. *Advances in neural information processing systems*, 32, 2019.
- [4] Ilyes Batatia, Simon Batzner, Dávid Péter Kovács, Albert Musaelian, Gregor NC Simm, Ralf Drautz, Christoph Ortner, Boris Kozinsky, and Gábor Csányi. The design space of  $e(3)$ -equivariant atom-centered interatomic potentials. *arXiv preprint arXiv:2205.06643*, 2022.
- [5] Ilyes Batatia, Mario Geiger, Jose Munoz, Tess Smidt, Lior Silberman, and Christoph Ortner. A general framework for equivariant neural networks on reductive lie groups. *Advances in Neural Information Processing Systems*, 36, 2024.
- [6] Ilyes Batatia, David P Kovacs, Gregor Simm, Christoph Ortner, and Gábor Csányi. Mace: Higher order equivariant message passing neural networks for fast and accurate force fields. *Advances in Neural Information Processing Systems*, 35:11423–11436, 2022.
- [7] Simon Batzner, Albert Musaelian, Lixin Sun, Mario Geiger, Jonathan P Mailoa, Mordechai Kornbluth, Nicola Molinari, Tess E Smidt, and Boris Kozinsky.  $E(3)$ -equivariant graph neural networks for data-efficient and accurate interatomic potentials. *Nature communications*, 13(1):2453, 2022.
- [8] Eduardo Bayro-Corrochano, Leo Reyes-Lozano, and Julio Zamora-Esquivel. Conformal geometric algebra for robotic vision. *Journal of Mathematical Imaging and Vision*, 24:55–81, 2006.
- [9] Erik J Bekkers. B-spline cnns on lie groups. *arXiv preprint arXiv:1909.12057*, 2019.
- [10] Uzair Aslam Bhatti, Zhou Ming-Quan, Huo Qing-Song, Sajid Ali, Aamir Hussain, Yan Yuhuan, Zhaoyuan Yu, Linwang Yuan, and Saqib Ali Nawaz. Advanced color edge detection using clifford algebra in satellite images. *IEEE Photonics Journal*, 13(2):1–20, 2021.

- [11] Anton Bochkarev, Yury Lysogorskiy, Christoph Ortner, Gábor Csányi, and Ralf Drautz. Multilayer atomic cluster expansion for semilocal interactions. *Physical Review Research*, 4(4):L042019, 2022.
- [12] Johannes Brandstetter, Rob Hesselink, Elise van der Pol, Erik J Bekkers, and Max Welling. Geometric and physical quantities improve e(3) equivariant message passing. *arXiv preprint arXiv:2110.02905*, 2021.
- [13] Johann Brehmer, Pim De Haan, Sönke Behrends, and Taco Cohen. Geometric algebra transformers. *arXiv preprint arXiv:2305.18415*, 2023.
- [14] Stephane Breuils, Kanta Tachibana, and Eckhard Hitzer. New applications of clifford’s geometric algebra. *Advances in Applied Clifford Algebras*, 32(2):17, 2022.
- [15] Joan Bruna, Wojciech Zaremba, Arthur Szlam, and Yann LeCun. Spectral networks and locally connected networks on graphs. *arXiv preprint arXiv:1312.6203*, 2013.
- [16] Stefan Chmiela, Alexandre Tkatchenko, Huziel E Sauceda, Igor Poltavsky, Kristof T Schütt, and Klaus-Robert Müller. Machine learning of accurate energy-conserving molecular force fields. *Science advances*, 3(5):e1603015, 2017.
- [17] CMU. Carnegie-mellon motion capture database, 2003.
- [18] Taco Cohen and Max Welling. Group equivariant convolutional networks. In *International conference on machine learning*, pages 2990–2999. PMLR, 2016.
- [19] Benjamin Coors, Alexandru Paul Condurache, and Andreas Geiger. Spherenet: Learning spherical representations for detection and classification in omnidirectional images. In *Proceedings of the European conference on computer vision (ECCV)*, pages 518–533, 2018.
- [20] Michaël Defferrard, Xavier Bresson, and Pierre Vandergheynst. Convolutional neural networks on graphs with fast localized spectral filtering. *Advances in neural information processing systems*, 29, 2016.
- [21] Congyue Deng, Or Litany, Yueqi Duan, Adrien Poulenard, Andrea Tagliasacchi, and Leonidas J Guibas. Vector neurons: A general framework for SO(3)-equivariant networks. In *Proceedings of the IEEE/CVF International Conference on Computer Vision*, pages 12200–12209, 2021.
- [22] Floor Eijkelboom, Rob Hesselink, and Erik J Bekkers. E(n) equivariant message passing simplicial networks. In *International Conference on Machine Learning*, pages 9071–9081. PMLR, 2023.
- [23] Jiarui Feng, Yixin Chen, Fuhai Li, Anindya Sarkar, and Muhan Zhang. How powerful are k-hop message passing graph neural networks. *Advances in Neural Information Processing Systems*, 35:4776–4790, 2022.

- [24] Marc Finzi, Samuel Stanton, Pavel Izmailov, and Andrew Gordon Wilson. Generalizing convolutional neural networks for equivariance to lie groups on arbitrary continuous data. In *International Conference on Machine Learning*, pages 3165–3176. PMLR, 2020.
- [25] Fabian Fuchs, Daniel Worrall, Volker Fischer, and Max Welling. Se (3)-transformers: 3d roto-translation equivariant attention networks. *Advances in neural information processing systems*, 33:1970–1981, 2020.
- [26] D. J. H. Garling. *Clifford Algebras: An Introduction*. London Mathematical Society Student Texts. Cambridge University Press, 2011.
- [27] Johannes Gasteiger, Florian Becker, and Stephan Günnemann. Gemnet: Universal directional graph neural networks for molecules. *Advances in Neural Information Processing Systems*, 34:6790–6802, 2021.
- [28] Johannes Gasteiger, Janek Groß, and Stephan Günnemann. Directional message passing for molecular graphs. *arXiv preprint arXiv:2003.03123*, 2020.
- [29] Justin Gilmer, Samuel S Schoenholz, Patrick F Riley, Oriol Vinyals, and George E Dahl. Neural message passing for quantum chemistry. In *International conference on machine learning*, pages 1263–1272. PMLR, 2017.
- [30] Justin Gilmer, Samuel S. Schoenholz, Patrick F. Riley, Oriol Vinyals, and George E. Dahl. Neural message passing for quantum chemistry. In Doina Precup and Yee Whye Teh, editors, *Proceedings of the 34th International Conference on Machine Learning*, volume 70 of *Proceedings of Machine Learning Research*, pages 1263–1272. PMLR, 06–11 Aug 2017.
- [31] Hermann Grassmann. *Die Ausdehnungslehre*, volume 1. Enslin, 1862.
- [32] William Rowan Hamilton. *Elements of quaternions*. Longmans, Green, & Company, 1866.
- [33] Jiaqi Han, Wenbing Huang, Tingyang Xu, and Yu Rong. Equivariant graph hierarchy-based neural networks. *Advances in Neural Information Processing Systems*, 35:9176–9187, 2022.
- [34] Jiaqi Han, Yu Rong, Tingyang Xu, and Wenbing Huang. Geometrically equivariant graph neural networks: A survey. *arXiv preprint arXiv:2202.07230*, 2022.
- [35] Jeff Henrikson. Completeness and total boundedness of the hausdorff metric. *MIT Undergraduate Journal of Mathematics*, 1(69-80):10, 1999.
- [36] Dietmar Hildenbrand, Julio Zamora, and Eduardo Bayro-Corrochano. Inverse kinematics computation in computer graphics and robotics using conformal geometric algebra. *Advances in applied Clifford algebras*, 18:699–713, 2008.



- [37] Eckhard Hitzer and Christian Perwass. Interactive 3d space group visualization with clucalc and the clifford geometric algebra description of space groups. *Advances in applied Clifford algebras*, 20:631–658, 2010.
- [38] Max Hodapp and Alexander Shapeev. Equivariant tensor networks. *arXiv preprint arXiv:2304.08226*, 2023.
- [39] Wenbing Huang, Jiaqi Han, Yu Rong, Tingyang Xu, Fuchun Sun, and Junzhou Huang. Equivariant graph mechanics networks with constraints. In *International Conference on Learning Representations*, 2022.
- [40] Bowen Jing, Stephan Eismann, Patricia Suriana, Raphael JL Townshend, and Ron Dror. Learning from protein structure with geometric vector perceptrons. *arXiv preprint arXiv:2009.01411*, 2020.
- [41] Thomas N Kipf and Max Welling. Semi-supervised classification with graph convolutional networks. *arXiv preprint arXiv:1609.02907*, 2016.
- [42] Johannes Klicpera, Florian Becker, and Stephan Günnemann. Gemnet: Universal directional graph neural networks for molecules. *arXiv e-prints*, pages arXiv–2106, 2021.
- [43] Jonas Köhler, Leon Klein, and Frank Noé. Equivariant flows: sampling configurations for multi-body systems with symmetric energies. *arXiv preprint arXiv:1910.00753*, 2019.
- [44] Jonas Köhler, Leon Klein, and Frank Noé. Equivariant flows: exact likelihood generative learning for symmetric densities. In *International conference on machine learning*, pages 5361–5370. PMLR, 2020.
- [45] Risi Kondor and Shubhendu Trivedi. On the generalization of equivariance and convolution in neural networks to the action of compact groups. In *International Conference on Machine Learning*, pages 2747–2755. PMLR, 2018.
- [46] Cong Liu, David Ruhe, Floor Eijkelboom, and Patrick Forré. Clifford group equivariant simplicial message passing networks. *International Conference on Learning Representations*, 2024.
- [47] Ilya Loshchilov and Frank Hutter. Sgdr: Stochastic gradient descent with warm restarts. *arXiv preprint arXiv:1608.03983*, 2016.
- [48] Haggai Maron, Heli Ben-Hamu, Hadar Serviansky, and Yaron Lipman. Provably powerful graph networks. *Advances in neural information processing systems*, 32, 2019.
- [49] Haggai Maron, Heli Ben-Hamu, Nadav Shamir, and Yaron Lipman. Invariant and equivariant graph networks. *Proceedings of the AAAI conference on artificial intelligence*, 33(01):4602–4609, 2018.

- [50] Haggai Maron, Ethan Fetaya, Nimrod Segol, and Yaron Lipman. On the universality of invariant networks. In *International conference on machine learning*, pages 4363–4371. PMLR, 2019.
- [51] Pavlo Melnyk, Michael Felsberg, and Mårten Wadenbäck. Embed me if you can: A geometric perceptron. In *Proceedings of the IEEE/CVF International Conference on Computer Vision*, pages 1276–1284, 2021.
- [52] Christopher Morris, Martin Ritzert, Matthias Fey, William L Hamilton, Jan Eric Lenssen, Gaurav Rattan, and Martin Grohe. Weisfeiler and leman go neural: Higher-order graph neural networks. In *Proceedings of the AAAI conference on artificial intelligence*, volume 33, pages 4602–4609, 2019.
- [53] Albert Musaelian, Simon Batzner, Anders Johansson, Lixin Sun, Cameron J Owen, Mordechai Kornbluth, and Boris Kozinsky. Learning local equivariant representations for large-scale atomistic dynamics. *Nature Communications*, 14(1):579, 2023.
- [54] Jigyasa Nigam, Sergey Pozdnyakov, Guillaume Fraux, and Michele Ceriotti. Unified theory of atom-centered representations and message-passing machine-learning schemes. *The Journal of Chemical Physics*, 156(20), 2022.
- [55] Allan Pinkus. Approximation theory of the mlp model in neural networks. *Acta numerica*, 8:143–195, 1999.
- [56] Sergey N Pozdnyakov and Michele Ceriotti. Incompleteness of graph neural networks for points clouds in three dimensions. *Machine Learning: Science and Technology*, 3(4):045020, 2022.
- [57] David Ruhe, Johannes Brandstetter, and Patrick Forré. Clifford group equivariant neural networks. In *Thirty-seventh Conference on Neural Information Processing Systems*, 2023.
- [58] Victor Garcia Satorras, Emiel Hoogeboom, and Max Welling. E (n) equivariant graph neural networks. In *International conference on machine learning*, pages 9323–9332. PMLR, 2021.
- [59] Kristof Schütt, Pieter-Jan Kindermans, Huziel Enoc Saucedo Felix, Stefan Chmiela, Alexandre Tkatchenko, and Klaus-Robert Müller. Schnet: A continuous-filter convolutional neural network for modeling quantum interactions. *Advances in neural information processing systems*, 30, 2017.
- [60] Kristof Schütt, Oliver Unke, and Michael Gastegger. Equivariant message passing for the prediction of tensorial properties and molecular spectra. In *International Conference on Machine Learning*, pages 9377–9388. PMLR, 2021.
- [61] Kristof T Schütt, Huziel E Saucedo, P-J Kindermans, Alexandre Tkatchenko, and K-R Müller. Schnet—a deep learning architecture for molecules and materials. *The Journal of Chemical Physics*, 148(24), 2018.

- [62] Wen Shen, Zihua Wei, Qihan Ren, Binbin Zhang, Shikun Huang, Jiaqi Fan, and Quanshi Zhang. Rotation-equivariant quaternion neural networks for 3d point cloud processing. *IEEE Transactions on Pattern Analysis and Machine Intelligence*, 2024.
- [63] Wen Shen, Binbin Zhang, Shikun Huang, Zihua Wei, and Quanshi Zhang. 3d-rotation-equivariant quaternion neural networks. In *Computer Vision—ECCV 2020: 16th European Conference, Glasgow, UK, August 23–28, 2020, Proceedings, Part XX 16*, pages 531–547. Springer, 2020.
- [64] Matthew Spellings. Geometric algebra attention networks for small point clouds. *arXiv preprint arXiv:2110.02393*, 2021.
- [65] Philipp Thölke and Gianni De Fabritiis. Torchmd-net: equivariant transformers for neural network based molecular potentials. *arXiv preprint arXiv:2202.02541*, 2022.
- [66] Nathaniel Thomas, Tess Smidt, Steven Kearnes, Lusann Yang, Li Li, Kai Kohlhoff, and Patrick Riley. Tensor field networks: Rotation-and translation-equivariant neural networks for 3d point clouds. *arXiv preprint arXiv:1802.08219*, 2018.
- [67] Thuan Anh Trang, Nhat Khang Ngo, Daniel T Levy, Thieu Ngoc Vo, Siamak Ravanbakhsh, and Truong Son Hy. E (3)-equivariant mesh neural networks. In *International Conference on Artificial Intelligence and Statistics*, pages 748–756. PMLR, 2024.
- [68] Rich Wareham, Jonathan Cameron, and Joan Lasenby. Applications of conformal geometric algebra in computer vision and graphics. In *International Workshop on Mathematics Mechanization*, pages 329–349. Springer, 2004.
- [69] Keyulu Xu, Weihua Hu, Jure Leskovec, and Stefanie Jegelka. How powerful are graph neural networks? *arXiv preprint arXiv:1810.00826*, 2018.
- [70] Yongheng Zhao, Tolga Birdal, Jan Eric Lenssen, Emanuele Menegatti, Leonidas Guibas, and Federico Tombari. Quaternion equivariant capsule networks for 3d point clouds. In *European conference on computer vision*, pages 1–19. Springer, 2020.

# Supplement to “Monomial Matrix Group Equivariant Neural Functional Networks”

## Appendix A. Introduction of Clifford Group and Clifford Group Equivariant Neural Networks

For formal construction and details, see Appendix B, [26] and [57].

### Appendix A.1. Clifford Algebra

Let  $(V, \mathfrak{q})$  be an  $n$ -dimensional quadratic space over a field  $\mathbb{F}$  with  $\text{char } \mathbb{F} \neq 2$ . The Clifford Algebra, denoted by  $\text{Cl}(V, \mathfrak{q})$ , is the  $\mathbb{F}$ -algebra generated by  $V$  with relations  $v^2 = \mathfrak{q}(v)$  for all  $v \in V$ , i.e. every element of  $\text{Cl}(V, \mathfrak{q})$  is a linear combination of formal products of vectors in  $V$  modulo that relation: For all  $x \in \text{Cl}(V, \mathfrak{q})$ :

$$x = \sum_{i \in I} c_i \cdot v_{i,1} \cdots v_{i,k_i}, \quad (\text{A.1})$$

where  $I$  is finite,  $c \in \mathbb{F}$ ,  $v_{i,j} \in V$ .  $\text{Cl}(V, \mathfrak{q})$  is an  $2^n$ -dimensional vector space and it has a decomposition into  $n + 1$  subspace  $\text{Cl}^{(m)}(V, \mathfrak{q})$ ,  $m = 0, \dots, n$ , called grades:

$$\text{Cl}(V, \mathfrak{q}) = \bigoplus_{m=0}^n \text{Cl}^{(m)}(V, \mathfrak{q}) \quad (\text{A.2})$$

We have  $\dim_{\mathbb{F}}(\text{Cl}^{(m)}(V, \mathfrak{q})) = \binom{n}{m}$ . The field  $\mathbb{F}$  and the space  $V$  can be identified as  $\text{Cl}^{(0)}(V, \mathfrak{q})$  and  $\text{Cl}^{(1)}(V, \mathfrak{q})$ , respectively. Denote the parity decomposition of  $x \in \text{Cl}(V, \mathfrak{q})$  as  $x = x^{[0]} + x^{[1]}$ , where  $x^{[i]} \in \bigoplus_{0 \leq m \leq n}^{\substack{m \equiv i \pmod{2}}} \text{Cl}^{(m)}(V, \mathfrak{q}) = \text{Cl}^{[i]}(V, \mathfrak{q})$  for  $i = 0, 1$ .

Let  $\text{Cl}^\times(V, \mathfrak{q})$  denote the group of invertible elements of  $\text{Cl}(V, \mathfrak{q})$ . Each  $w \in \text{Cl}^\times(V, \mathfrak{q})$  defines an endomorphism of  $\text{Cl}(V, \mathfrak{q})$  via the (adjusted) twisted conjugation:

$$\begin{aligned} \rho(w): \text{Cl}(V, \mathfrak{q}) &\longrightarrow \text{Cl}(V, \mathfrak{q}) \\ x &\longmapsto wx^{[0]}w^{-1} + \alpha(w)x^{[1]}w^{-1}, \end{aligned} \quad (\text{A.3})$$

where  $\alpha$  is the main involution of  $\text{Cl}(V, \mathfrak{q})$ , which is given by  $\alpha(w) := x^{[0]} - x^{[1]}$ . The Clifford group, denoted by  $\Gamma(V, \mathfrak{q})$ , is a subgroup of  $\text{Cl}^\times(V, \mathfrak{q})$  consists of elements that is parity homogeneous and preserves  $V$  via  $\rho$ :

$$\Gamma(V, \mathfrak{q}) = \left\{ w \in \text{Cl}^\times(V, \mathfrak{q}) \cap \left( \text{Cl}^{[0]}(V, \mathfrak{q}) \cup \text{Cl}^{[1]}(V, \mathfrak{q}) \right) \mid \rho(V) \subset V \right\}. \quad (\text{A.4})$$

We can show that for  $w \in \Gamma(V, \mathfrak{q})$ ,  $\rho(w)$  is an automorphism of  $\text{Cl}(V, \mathfrak{q})$  and preserves each subspace  $\text{Cl}^{(m)}(V, \mathfrak{q})$ . This means  $\text{Cl}(V, \mathfrak{q})$  and  $\text{Cl}^{(m)}(V, \mathfrak{q})$  are group representations of  $\Gamma(V, \mathfrak{q})$  (via  $\rho$ ). On other hand, the orthogonal group

of  $(V, \mathfrak{q})$  consists of linear automorphisms of  $V$  that preserve quadratic form  $\mathfrak{q}$ , which is:

$$\mathrm{O}(V, \mathfrak{q}) = \left\{ \text{linear automorphism } f \text{ of } V \mid \forall v \in V, \mathfrak{q}(f(v)) = \mathfrak{q}(v) \right\}. \quad (\text{A.5})$$

Assume that  $(V, \mathfrak{q})$  is non-degenerate. By a theorem of Cartan-Dieudonné about every orthogonal transformation in an  $n$ -dimensional symmetric bilinear space is composition of at most  $n$  reflections, we can show that  $\mathrm{O}(V, \mathfrak{q})$  can be identified as the Clifford group  $\Gamma(V, \mathfrak{q})$  up to multiplication by an invertible scalar. Formally, we have an exact sequence (note that, by A.3,  $\rho(w) = \mathrm{id}_{\mathrm{Cl}(V, \mathfrak{q})}$  for all  $w \in \mathbb{F}^\times$ ):

$$0 \longrightarrow \mathbb{F}^\times \xleftarrow{i} \Gamma(V, \mathfrak{q}) \xrightarrow{\rho|_V} \mathrm{O}(V, \mathfrak{q}) \longrightarrow 0. \quad (\text{A.6})$$

For  $w \in \Gamma(V, \mathfrak{q})$ , we have  $f = \rho|_V \in \mathrm{O}(V, \mathfrak{q})$  defines an automorphism of  $\mathrm{Cl}(V, \mathfrak{q})$  by  $\rho(w)$ . Consider  $x$  in Eq. (A.1):

$$\begin{aligned} \rho(w)(x) &= \sum_{i \in I} c_i \cdot \rho(w)(v_{i,1}) \cdots \rho(w)(v_{i,k_i}) \\ &= \sum_{i \in I} c_i \cdot f(v_{i,1}) \cdots f(v_{i,k_i}). \end{aligned} \quad (\text{A.7})$$

So  $\rho$  also defines a representation of  $\mathrm{O}(V, \mathfrak{q})$  on  $\mathrm{Cl}(V, \mathfrak{q})$  which is identical with  $\Gamma(V, \mathfrak{q})$  up to multiplication of invertible scalar. Its subrepresentation on  $\mathrm{Cl}^{(0)}(V, \mathfrak{q})$  and  $\mathrm{Cl}^{(1)}(V, \mathfrak{q})$  is identity and the canonical representation of  $\mathrm{O}(V, \mathfrak{q})$  on  $V$ .

#### Appendix A.2. Clifford Group Equivariant Neural Networks (CGENNs)

In context of equivariance, one important result in [57] is grade projections and polynomials with coefficients in  $\mathbb{F}$  are  $\Gamma(V, \mathfrak{q})$ -equivariant. [57] also provides some  $\Gamma(V, \mathfrak{q})$ -equivariant layers constructed by these maps, which are linear layer, (fully-connected) geometric product layer, normalization layer and nonlinear activation. Details of these layers can be found in Appendix Appendix C. Using those layers, we can design  $\Gamma(V, \mathfrak{q})$ -equivariant neural networks, which we will call Clifford networks. Finally, we can optionally embed the input or take grade projection of output to induce neural networks that are  $\mathrm{O}(n)$ -equivariant.

For the rest of this paper, denote  $\mathrm{Cl}(\mathbb{R}^n)$  as the Clifford algebra of the  $n$ -dimensional real vector space  $\mathbb{R}^n$  with quadratic form  $\mathfrak{q}$  is the square of the Euclidean norm, i.e.  $\mathfrak{q}(\cdot) = \|\cdot\|_2^2$ . In this case, the orthogonal group of  $\mathrm{O}(\mathbb{R}^n, \|\cdot\|_2^2)$  is the orthogonal group  $\mathrm{O}(n)$ :

$$\mathrm{O}(n) = \{Q \in \mathrm{GL}(n) \mid Q^\top Q = QQ^\top = I_n\}. \quad (\text{A.8})$$

By identifying  $\mathrm{O}(n) \simeq \Gamma(\mathbb{R}^n, \|\cdot\|_2^2)/\mathbb{R}^\times$  from Eq. (A.6), we say that  $\mathrm{O}(n)$  acts on  $\mathrm{Cl}(\mathbb{R}^n)$  by Eq. (A.7).

## Appendix B. Clifford Algebra

We follow [57] and [26]. Let  $\mathbb{F}$  denote a field with  $\text{char } \mathbb{F} \neq 2$ . Let  $V$  be a vector space over  $\mathbb{F}$  of finite dimension  $\dim_{\mathbb{F}} V = n$ .

### Appendix B.1. Clifford Algebra

**Definition Appendix B.1** (Quadratic forms and quadratic vector spaces). A map  $\mathfrak{q}: V \rightarrow \mathbb{F}$  is called a *quadratic form* of  $V$  if for all  $c \in \mathbb{F}$  and  $v, v_1, v_2 \in V$ , we have:

$$\mathfrak{q}(c \cdot v) = c^2 \cdot \mathfrak{q}(v). \quad (\text{B.1})$$

In this case, the map  $\mathfrak{b}: V \times V \rightarrow \mathbb{F}$ , defined by:

$$\mathfrak{b}(v_1, v_2) := \frac{1}{2} (\mathfrak{q}(v_1 + v_2) - \mathfrak{q}(v_1) - \mathfrak{q}(v_2)), \quad (\text{B.2})$$

is a bilinear form over  $\mathbb{F}$ . The tuple  $(V, \mathfrak{q})$  will be called a *quadratic space*. We have a bijective correspondence between *quadratic forms* and *symmetric bilinear forms* on  $V$ .

**Definition Appendix B.2** (Orthogonal basis). A basis  $e_1, \dots, e_n$  of  $V$  is called an *orthogonal basis* of  $V$  if for all  $i \neq j$  we have:

$$\mathfrak{b}(e_i, e_j) = 0. \quad (\text{B.3})$$

It is called an *orthonormal basis* if, in addition,  $\mathfrak{q}(e_i) \in \{-1, 0, 1\}$  for all  $i = 1, \dots, n$ .

**Definition Appendix B.3** (Clifford algebra). Define the *Clifford algebra*  $\text{Cl}(V, \mathfrak{q})$  as the quotient of the tensor algebra of  $V$ :

$$\text{T}(V) := \bigoplus_{m=0}^{\infty} V^{\otimes m} = \bigoplus_{m=0}^{\infty} \text{span}\{v_1 \otimes \dots \otimes v_m \mid v_1, \dots, v_m \in V\}, \quad (\text{B.4})$$

by the ideal

$$I(V, \mathfrak{q}) := \langle v \otimes v - \mathfrak{q} \cdot 1_{\text{T}(V)} \mid v \in V \rangle, \quad (\text{B.5})$$

which is  $\text{Cl}(V, \mathfrak{q}) := \text{T}(V)/I(V, \mathfrak{q})$ . Denote the canonical quotient map as  $\pi: \text{T}(V) \rightarrow \text{Cl}(V, \mathfrak{q})$ .

The quadratic form  $\mathfrak{q}$  and the bilinear form  $\mathfrak{b}$  can be canonically extended to  $\text{Cl}(V, \mathfrak{q})$ , so we can define the orthogonality on  $\text{Cl}(V, \mathfrak{q})$ .

**Theorem Appendix B.4** (Basis of Clifford algebra). *If  $e_1, \dots, e_n$  is any basis of  $(V, \mathfrak{q})$  then  $(e_A)_{A \subseteq [n]}$  is a basis for  $\text{Cl}(V, \mathfrak{q})$ , where for  $A \subseteq [n]$ :*

$$e_A := \prod_{i \in A}^< e_i, \quad (\text{B.6})$$

where the product is taken in increasing order of the indices  $i \in A$ .

In other words,  $\dim_{\mathbb{R}} \text{Cl}(V, \mathfrak{q}) = 2^n$ . Moreover, if  $(e_i)_{i \in [n]}$  is an orthogonal basis of  $V$ ,  $(e_A)_{A \subseteq [n]}$  is an orthogonal basis of  $\text{Cl}(V, \mathfrak{q})$ .

**Theorem Appendix B.5** (The multivector grading of the Clifford algebra). *Let  $e_1, \dots, e_n$  be an orthogonal basis of  $(V, \mathfrak{q})$ . Then for every  $m = 0, \dots, n$  we define the following vector subspace of  $\text{Cl}(V, \mathfrak{q})$ :*

$$\text{Cl}^{(m)}(V, \mathfrak{q}) := \text{span}\{e_A \mid A \subseteq [n], |A| = m\}. \quad (\text{B.7})$$

*Then the vector subspaces  $\text{Cl}^{(m)}(V, \mathfrak{q})$ ,  $m = 0, \dots, n$ , are independent of the choice of the orthogonal basis. One has  $\dim_{\mathbb{F}}(\text{Cl}^{(m)}(V, \mathfrak{q})) = \binom{n}{m}$ . Also,  $\text{Cl}^{(m)}(V, \mathfrak{q})$  is the space of all elements of degree  $m$ .*

The direct sum

$$\text{Cl}(V, \mathfrak{q}) = \bigoplus_{m=0}^n \text{Cl}^{(m)}(V, \mathfrak{q}), \quad (\text{B.8})$$

is an orthogonal sum. We write  $x \in \text{Cl}(V, \mathfrak{q})$  as  $x = x^{(0)} + x^{(1)} + \dots + x^{(n)}$ , where  $x^{(m)} \in \text{Cl}^{(m)}(V, \mathfrak{q})$  denotes the grade- $m$  part of  $x$ . Define

$$\text{Cl}^{[0]}(V, \mathfrak{q}) := \bigoplus_{m \text{ even}}^n \text{Cl}^{(m)}(V, \mathfrak{q}), \quad \text{Cl}^{[1]}(V, \mathfrak{q}) := \bigoplus_{m \text{ odd}}^n \text{Cl}^{(m)}(V, \mathfrak{q}), \quad (\text{B.9})$$

where elements of even and odd parity, respectively. We also have an orthogonal decomposition of  $\text{Cl}(V, \mathfrak{q})$  which is the parity decomposition:

$$\text{Cl}(V, \mathfrak{q}) = \text{Cl}^{[0]}(V, \mathfrak{q}) \bigoplus \text{Cl}^{[1]}(V, \mathfrak{q}). \quad (\text{B.10})$$

We write  $x \in \text{Cl}(V, \mathfrak{q})$  as  $x = x^{[0]} + x^{[1]}$ , where  $x^{[i]} \in \text{Cl}^{[i]}(V, \mathfrak{q})$ , to denote the *parity decomposition* of  $x$ .

#### Appendix B.2. Clifford Group

Let  $\text{Cl}^\times(V, \mathfrak{q})$  denote the group of invertible elements of the Clifford algebra. For  $w \in \text{Cl}^\times(V, \mathfrak{q})$ , we defined the (*adjusted*) *twisted conjugation*:

$$\begin{aligned} \rho(w): \text{Cl}(V, \mathfrak{q}) &\longrightarrow \text{Cl}(V, \mathfrak{q}) \\ x &\longmapsto wx^{[0]}w^{-1} + \alpha(w)x^{[1]}w^{-1}, \end{aligned} \quad (\text{B.11})$$

where  $\alpha$  is the *main involution* of  $\text{Cl}^\times(V, \mathfrak{q})$ , which is given by  $\alpha(w) := w^{[0]} - w^{[1]}$ . The *Clifford group*, denoted by  $\Gamma(V, \mathfrak{q})$ , is a subgroup of  $\text{Cl}^\times(V, \mathfrak{q})$  consists of elements that is parity homogeneous and preserves  $V$  via  $\rho$ :

$$\Gamma(V, \mathfrak{q}) = \left\{ w \in \text{Cl}^\times(V, \mathfrak{q}) \cap \left( \text{Cl}^{[0]}(V, \mathfrak{q}) \cup \text{Cl}^{[1]}(V, \mathfrak{q}) \right) \mid \rho(V) \subset V \right\}. \quad (\text{B.12})$$

**Proposition Appendix B.6.** 1. *For  $w \in \mathbb{F}^\times$ , we have  $w \in \Gamma(V, \mathfrak{q})$  and  $\rho(w) = \text{id}_{\text{Cl}(V, \mathfrak{q})}$ .*

2. *For  $w \in V$  with  $\mathfrak{q}(w) \neq 0$ , we have  $w \in \Gamma(V, \mathfrak{q})$  and  $\rho(w)|_V$  is the reflection onto the hyperplane that is normal to  $w$ .  $\rho(w)$  is given by the following formula: For  $v \in V$ :*

$$\rho(w)(v) = v - 2 \frac{\mathfrak{b}(w, v)}{\mathfrak{b}(w, w)} w. \quad (\text{B.13})$$

**Theorem Appendix B.7.** *The map*

$$\begin{aligned} \rho: \Gamma(V, \mathfrak{q}) &\longrightarrow \text{Aut}_{\mathbf{Alg}, \text{grad}}(\text{Cl}(V, \mathfrak{q})) \\ w &\longmapsto \rho(w), \end{aligned} \quad (\text{B.14})$$

*is a well-defined group homomorphism from the Clifford group to the group of  $\mathbb{F}$ -algebra automorphisms of  $\text{Cl}(V, \mathfrak{q})$  that preserve the multivector grading of  $\text{Cl}(V, \mathfrak{q})$ . In particular,  $\text{Cl}(V, \mathfrak{q})$  and  $\text{Cl}^{(m)}(V, \mathfrak{q})$  for  $m = 0, 1, \dots, n$  are group representations of  $\Gamma(V, \mathfrak{q})$  via  $\rho$ .*

*Moreover, each  $\rho(w)$  generates an orthogonal map with respect to the (extended) bilinear form  $\mathfrak{b}$ .*

**Theorem Appendix B.8** (All grade projections are Clifford group equivariant). *For  $w \in \Gamma(V, \mathfrak{q}), x \in \text{Cl}(V, \mathfrak{q})$  and  $m = 0, 1, \dots, n$  we have the following equivariance property:*

$$\rho(w)(x^{(m)}) = (\rho(w)(x))^{(m)}. \quad (\text{B.15})$$

**Theorem Appendix B.9** (All polynomials are Clifford group equivariant). *Let  $F \in \mathbb{F}[T_1, \dots, T_l]$  be a polynomial in  $l$  variables with coefficients in  $\mathbb{F}$ . Consider  $w \in \Gamma(V, \mathfrak{q})$  and  $l$  elements  $x_1, \dots, x_l \in \text{Cl}(V, \mathfrak{q})$ . We have the following equivariance property:*

$$\rho(w)(F(x_1, \dots, x_l)) = F(\rho(w)(x_1), \dots, \rho(w)(x_l)). \quad (\text{B.16})$$

*Appendix B.3. Orthogonal Group and its Action on Clifford Algebra*

**Definition Appendix B.10** (Orthogonal group). Define the *orthogonal group* of  $(V, \mathfrak{q})$  as

$$\text{O}(V, \mathfrak{q}) = \left\{ \text{linear automorphism } f \text{ of } V \mid \forall v \in V, \mathfrak{q}(f(v)) = \mathfrak{q}(v) \right\}. \quad (\text{B.17})$$

**Theorem Appendix B.11** (Theorem of Cartan-Dieudonné). *Let  $(V, \mathfrak{q})$  be a non-degenerate quadratic space of finite dimension  $\dim V = n$  over a field  $\mathbb{F}$  of char  $\mathbb{F} \neq 2$ . Then every element  $g \in \text{O}(V, \mathfrak{q})$  can be written as:*

$$g = r_1 \circ \dots \circ r_k, \quad (\text{B.18})$$

*where  $0 \leq k \leq n$  and  $r_i$ 's are reflections with respect to non-singular hyperplanes.*

**Theorem Appendix B.12.** *If  $(V, \mathfrak{q})$  is non-degenerate then we have a short exact sequence:*

$$0 \longrightarrow \mathbb{F}^\times \xrightarrow{i} \Gamma(V, \mathfrak{q}) \xrightarrow{\rho|_V} \text{O}(V, \mathfrak{q}) \longrightarrow 0. \quad (\text{B.19})$$

*In particular, one has  $\Gamma(V, \mathfrak{q})/\mathbb{F}^\times \simeq \text{O}(V, \mathfrak{q})$ .*



The above implies that  $O(V, \mathfrak{q})$  acts on whole  $\text{Cl}(V, \mathfrak{q})$  in a well-defined way. Concretely, if  $x \in \text{Cl}(V, \mathfrak{q})$  is of the form  $x = \sum_{i \in I} c_i \cdot v_{i,1} \cdots v_{i,k_i}$  with  $v_{i,j} \in V, c_i \in \mathbb{F}$  and  $f \in O(V, \mathfrak{q})$  corresponds to  $[w] \in \Gamma(V, \mathfrak{q})/\mathbb{F}^\times$ , then:

$$\rho(w)(x) = \sum_{i \in I} c_i \cdot \rho(w)(v_{i,1}) \cdots \rho(w)(v_{i,k_i}) = \sum_{i \in I} c_i \cdot f(v_{i,1}) \cdots f(v_{i,k_i}). \quad (\text{B.20})$$

**Theorem Appendix B.13.** *A map  $f: \text{Cl}(V, \mathfrak{q})^p \rightarrow \text{Cl}(V, \mathfrak{q})^q$  is equivariant to the Clifford group  $\Gamma(V, \mathfrak{q})$  if and only if it is equivariant to the orthogonal group  $O(V, \mathfrak{q})$ .*

#### Appendix B.4. Finite Dimensional Real Vector Space with Euclidean norm

In this subsection, we only consider the case  $\mathbb{F} = \mathbb{R}$  is the field of real numbers, and  $V$  is an  $n$ -dimensional vector space over  $\mathbb{R}$  with the quadratic form  $\mathfrak{q}$  is the square of the Euclidean norm, i.e.  $\mathfrak{q}(\cdot) = \|\cdot\|_2^2$ . In this case,  $(V, \mathfrak{q})$  a quadratic space that is non-degenerate. The orthogonal group  $O(V, \mathfrak{q})$  now is the usual orthogonal group  $O(n)$ .

**Proposition Appendix B.14.**  *$(V, \mathfrak{q})$  has an orthonormal basis.*

**Proposition Appendix B.15.** *For  $w \in V, w \neq 0$ ,  $\rho(w)$  defines the reflection of  $V$  onto the hyperplane that is normal to  $w$ .*

**Proposition Appendix B.16.** *The Clifford group  $\Gamma(V, \mathfrak{q})$  can be defined by:*

$$\Gamma(V, \mathfrak{q}) = \{c \cdot v_1 \cdots v_k \mid c \in \mathbb{R}^\times, k \geq 0, v_i \in V, v_i \neq 0\} \quad (\text{B.21})$$

$$= \{c \cdot v_1 \cdots v_k \mid c \in \mathbb{R}^\times, 0 \leq k \leq n, v_i \in V, v_i \neq 0\}. \quad (\text{B.22})$$

## Appendix C. Clifford Group Equivariant Layers

This section provides a way to design a neural network where neurons are elements of Clifford Algebra  $\text{Cl}(V, \mathfrak{q})$  and equivariant under the action of the Clifford group  $\Gamma(V, \mathfrak{q})$ . Each layer has the form as follows:

$$\mathbf{T}_\Phi: \text{Cl}(V, \mathfrak{q})^p \rightarrow \text{Cl}(V, \mathfrak{q})^q, \quad x = (x_1, \dots, x_p) \mapsto y = (y_1, \dots, y_q), \quad (\text{C.1})$$

where  $p, q$  represent the number of input and output channels, respectively, and  $\Phi = (\phi_-)$  is a learnable hyperparameter.

**Definition Appendix C.1** (Linear Layer). The *linear layer*  $\mathbf{T}_\Phi^{\text{lin}}: \text{Cl}(V, \mathfrak{q})^p \rightarrow \text{Cl}(V, \mathfrak{q})^q$  is defined as follows:

$$y_{c_{\text{out}}}^{(k)} := \sum_{c_{\text{in}}=1}^p \phi_{c_{\text{out}}, c_{\text{in}}, k} \cdot x_{c_{\text{in}}}^{(k)}, \quad \forall c_{\text{out}} = 1, \dots, q. \quad (\text{C.2})$$

**Definition Appendix C.2** (Geometric Product Layer). The interaction between two elements of Clifford Algebra is defined as follows:

$$\mathbf{P}_\Phi: \text{Cl}(V, \mathfrak{q}) \times \text{Cl}(V, \mathfrak{q}) \rightarrow \text{Cl}(V, \mathfrak{q}), \quad \mathbf{P}_\Phi(x, \tilde{x})^{(k)} = \sum_{i=0}^n \sum_{j=0}^n \phi_{i,j,k} \cdot \left( x^{(i)} \tilde{x}^{(j)} \right)^{(k)}. \quad (\text{C.3})$$

We first apply a linear map to input  $x = (x_1, \dots, x_p) \in \text{Cl}(V, \mathfrak{q})^p$  to obtain  $z = (z_1, \dots, z_p) \in \text{Cl}(V, \mathfrak{q})^p$ .

The *geometric product layer*  $\mathbf{T}_\Phi^{\text{prod}}: \text{Cl}(V, \mathfrak{q})^p \rightarrow \text{Cl}(V, \mathfrak{q})^p$  is defined as follows:

$$y_{c_{\text{out}}}^{(k)} := \mathbf{P}_{\phi_{c_{\text{out}}}}(x_{c_{\text{out}}}, z_{c_{\text{out}}})^{(k)}, \quad \forall c_{\text{out}} = 1, \dots, p. \quad (\text{C.4})$$

The *fully-connected geometric product layer*  $\mathbf{T}_\Phi^{\text{prod}}: \text{Cl}(V, \mathfrak{q})^p \rightarrow \text{Cl}(V, \mathfrak{q})^p$  is defined as follows:

$$y_{c_{\text{out}}}^{(k)} := \sum_{c_{\text{in}}=1}^p \mathbf{P}_{\phi_{c_{\text{out}}, c_{\text{in}}}}(x_{c_{\text{in}}}, z_{c_{\text{in}}})^{(k)}, \quad \forall c_{\text{out}} = 1, \dots, p. \quad (\text{C.5})$$

**Definition Appendix C.3** (Normalization Layer). The *normalization layer*  $\mathbf{T}_\Phi^{\text{norm}}: \text{Cl}(V, \mathfrak{q}) \rightarrow \text{Cl}(V, \mathfrak{q})$  is defined as follows:

$$x_{\text{out}}^{(m)} = \frac{x_{\text{in}}^{(m)}}{\sigma(\phi_m) \left( \mathfrak{q} \left( x_{\text{in}}^{(m)} \right) - 1 \right) + 1}, \quad \forall m = 0, 1, \dots, n. \quad (\text{C.6})$$

Here,  $\sigma$  denotes the sigmoid function.

**Definition Appendix C.4** (Nonlinear Activation). The *nonlinear activation*  $\mathbf{T}^{\text{non-lin}}: \text{Cl}(V, \mathfrak{q}) \rightarrow \text{Cl}(V, \mathfrak{q})$  is defined as follows:

$$x_{\text{out}}^{(0)} = \text{ReLU} \left( x_{\text{in}}^{(0)} \right) \quad \text{and} \quad x_{\text{out}}^{(m)} = \sigma \left( \mathfrak{q} \left( x_{\text{in}}^{(m)} \right) \right) x_{\text{in}}^{(m)}. \quad (\text{C.7})$$

Here,  $\sigma$  denotes the sigmoid function. Note that, the nonlinear activation does not require learnable hyperparameter.

The maps in the above definitions are equivariant to the Clifford group, by Theorem. Appendix B.8 and Theorem. Appendix B.9.

## Appendix D. Equivariance Proof for CG-EGNNs

We provide a proof for Theorem 4.2 and also Theorem 4.5 that we recall below by:

$$Q \cdot \mathbf{x}_i^L + g = \text{CG-EGNN}(Q \cdot \mathbf{x}_i + g), \quad (\text{D.1})$$

for all orthogonal matrix  $Q \in O(n)$ , translation vector  $g \in \mathbb{R}^n$  and  $i = 1, \dots, M$ .

For  $\mathbf{x} = \{\mathbf{x}_1, \dots, \mathbf{x}_M\}$ , denote the mean-subtracted positions of  $\mathbf{x}$  as follows:

$$\bar{\mathbf{x}} = \{\bar{\mathbf{x}}_1, \dots, \bar{\mathbf{x}}_M\}, \quad (\text{D.2})$$

where

$$\bar{\mathbf{x}}_i = \mathbf{x}_i - \frac{1}{M} \sum_{j=1}^M \mathbf{x}_j, \forall i = 1, \dots, M. \quad (\text{D.3})$$

Now, we analyze CG-EGNN. Removing the residual connection and decomposing as follows:

$$\Psi := \text{CG-EGNN (without residual connection)} \quad (\text{D.4})$$

$$= \text{Projection} \circ \underbrace{\text{Convolution} \circ \dots \circ \text{Convolution}}_{L \text{ times}} \circ \text{Embedding}. \quad (\text{D.5})$$

Each map **Embedding**, **Convolution**, **Projection** is constructed by the layers presented in Appendix Appendix C, so they are  $O(n)$ -equivariant. So composition of them is  $O(n)$ -equivariant. Now we have:

$$\begin{aligned} \text{CG-EGNN}(Q \cdot \mathbf{x}_i + g) &= (Q \cdot \mathbf{x}_i + g) + \Psi(Q \cdot \mathbf{x}_i + g) \\ &= (Q \cdot \mathbf{x}_i + g) + \Psi(\overline{Q \cdot \mathbf{x}_i + g}) \\ &= (Q \cdot \mathbf{x}_i + g) + \Psi\left(Q \cdot \mathbf{x}_i + g - \frac{1}{M} \sum_{j=1}^M (Q \cdot \mathbf{x}_j + g)\right) \\ &= (Q \cdot \mathbf{x}_i + g) + \Psi\left(Q \cdot \left(\mathbf{x}_i - \frac{1}{M} \sum_{j=1}^M \mathbf{x}_j\right)\right) \\ &= (Q \cdot \mathbf{x}_i + g) + \Psi(Q \cdot \bar{\mathbf{x}}_i) \\ &= (Q \cdot \mathbf{x}_i + g) + Q \cdot \Psi(\bar{\mathbf{x}}_i) \\ &= (Q \cdot \mathbf{x}_i + g) + Q \cdot \Psi(\mathbf{x}_i) \\ &= Q \cdot (\mathbf{x} + \Psi(\mathbf{x}_i)) + g \\ &= Q \cdot \mathbf{x}_i^L + g. \end{aligned} \quad (\text{D.6})$$

The theorem is then proved.

## Appendix E. Proof of Theorem 5.1

We provide a proof for Theorem 5.1. Fix an arbitrary  $\epsilon > 0$ . Since  $\mathcal{X}$  is a compact metric space,  $f$  is uniformly continuous on  $\mathcal{X}$ . As a consequence, there exists  $\delta > 0$  such that: for arbitrary graphs  $G$  and  $G'$  in  $\mathcal{X}$ , we always have:

$$d_H(G, G') < \delta \Rightarrow \|f(G) - f(G')\|_\infty < \epsilon.$$

Set  $K > \max\{\lceil \frac{1}{\delta} \rceil, \lceil \frac{1}{3\alpha} \rceil\}$ . Here,  $\alpha$  is a positive number given in Eq. (17). Let  $\mathcal{R} = \{\frac{2i-1}{2K} \mid i = 1, \dots, K\}$  be the set of equidistance values in the interval  $[0, 1]$ . Then  $\mathcal{R}^d$  forms a lattice inside the  $d$ -dimensional box  $[0, 1]^d$ . For each point  $z \in \mathbb{R}^d$ , we define by  $\bar{z}$  to be the nearest point of  $z$  in the lattice  $\mathcal{R}^d$ . For each  $G \in \mathcal{X}$ , we set  $\bar{G} = \{\bar{z} \mid z \in G\}$  which is a finite set of points in the box  $\mathcal{R}^d$ .

According to the definition of  $K$ , different nodes of the same graph  $G$  in  $\mathcal{X}$  will have different images in  $\mathcal{R}^d$ . Then we have  $d_H(G, \bar{G}) < \delta$ , thus,

$$\|f(G) - f(\bar{G})\|_\infty < \epsilon. \quad (\text{E.1})$$

Next, we will find an alternative representation for  $f(\bar{G})$ . First, for each  $c \in \mathcal{R}^d$ , we define a function  $\delta_c: \mathbb{R}^d \rightarrow [0, 1]$  by:

$$\delta_c(z) = \frac{1 - e^{-d(z, \mathbb{R}^d \setminus B(c, \frac{1}{2K}))}}{1 - e^{-d(c, \mathbb{R}^d \setminus B(c, \frac{1}{2K}))}} \quad (\text{E.2})$$

for each  $z \in \mathbb{R}^d$ . Then  $\delta_c$  is a nonnegative continuous function on  $\mathbb{R}^d$  such that:

$$\delta_c(z) = \begin{cases} 1, & \text{if } z = c, \\ \in (0, 1], & \text{if } z \in B(c, \frac{1}{2K}), \\ 0, & \text{if } z \in \mathbb{R}^d \setminus B(c, \frac{1}{2K}). \end{cases} \quad (\text{E.3})$$

Next, we define a map  $\phi_m: \mathbb{R}^d \rightarrow [0, 1]^{\mathcal{R}^d}$  as:

$$\phi_m(z) = (\delta_c(z))_{c \in \mathcal{R}^d}, \quad \text{for each } z \in \mathbb{R}^d. \quad (\text{E.4})$$

Then  $\phi_m$  is a continuous function on  $\mathbb{R}^d$  such that  $\phi_m(\mathcal{R}^d) \subseteq \{0, 1\}^{\mathcal{R}^d}$ . We also define a map  $\tau: [0, 1]^{\mathcal{R}^d} \rightarrow 2^{[0, 1]^d}$  by:

$$\tau((\epsilon_c)_{c \in \mathcal{R}^d}) = \{c \in \mathcal{R}^d \mid \epsilon_c > 0\}, \quad (\text{E.5})$$

for each  $(\epsilon_c)_{c \in \mathcal{R}^d} \in [0, 1]^{\mathcal{R}^d}$ . Here,  $2^{[0, 1]^d}$  is the collection of all subsets of  $[0, 1]^d$ . We will need the following two claims:

**Claim 1.** For every graph  $G \in \mathcal{X}$  and  $c \in \mathcal{R}^d$ , we have  $\sum_{z \in G} \delta_c(z) > 0$  if and only if  $c \in \bar{G}$ .

Indeed, since  $\delta_c$  is a nonnegative function, we have  $\sum_{z \in G} \delta_c(z) > 0$  if and only if there exists  $z_0 \in G$  such that  $\delta_c(z_0) > 0$ . Moreover, it follows from the definition of  $\delta_c$  that  $\delta_c(z_0) > 0$  if and only if  $z_0 \in B(c, \frac{1}{2K})$ . But  $z_0 \in B(c, \frac{1}{2K})$  if and only if  $c = \bar{z}_0 \in \bar{G}$ . The claim is proved.

**Claim 2.** For every graph  $G \in \mathcal{X}$ , we have:

$$\tau\left(\sum_{z \in G} \phi_m(z)\right) = \bar{G}. \quad (\text{E.6})$$

Indeed, from the definition of  $\phi_m$  and  $\tau$ , we have:

$$\begin{aligned} \tau \left( \sum_{z \in G} \phi_m(z) \right) &= \tau \left( \sum_{z \in G} (\delta_c(z))_{c \in \mathcal{R}^d} \right) \\ &= \tau \left( \left( \sum_{z \in G} \delta_c(z) \right)_{c \in \mathcal{R}^d} \right) \\ &= \left\{ c \in \mathcal{R}^d \mid \sum_{z \in G} \delta_c(z) > 0 \right\}. \end{aligned} \quad (\text{E.7})$$

Therefore, according to Claim 1, we have  $\tau \left( \sum_{z \in G} \phi_m(z) \right) = \bar{G}$ . Claim 2 is then proved.

By using Claim 2 and Eq. (E.6), we obtain:

$$f(\bar{G}) = f \circ \tau \left( \sum_{z \in G} \phi_m(z) \right). \quad (\text{E.8})$$

Set  $N = |\mathcal{R}^d|$  and  $\phi_h = f \circ \tau$ . Here, in order to make the composition  $f \circ \tau$  well-defined, we can restrict the domain of  $\tau$  to a subset of  $[0, 1]^{\mathcal{R}^d} = [0, 1]^N$  such that its image via  $\tau$  is contained in  $\mathcal{X}$ . We can extend  $\phi_h$  to a continuous function on  $\mathbb{R}^N$ . Then:

$$f(\bar{G}) = \phi_h \left( \sum_{z \in G} \phi_m(z) \right). \quad (\text{E.9})$$

It follows from Eq. (E.1) that:

$$\left\| f(G) - \phi_h \left( \sum_{z \in G} \phi_m(z) \right) \right\|_{\infty} < \epsilon. \quad (\text{E.10})$$

The theorem is then proved.

## Appendix F. Implementation details

In this session, we describe the experiment details for all experiments in session 6. All settings for CG-EGNN are kept as similar to the baseline as possible to ensure a fair comparison. All experiments in this paper is performed on a single A100 GPU.

### Appendix F.1. N-body System

**Experimental settings.** For this experiment, we employ the source code provided by [57]<sup>2</sup> and follow the same settings in the paper. In which, the node

<sup>2</sup><https://github.com/DavidRuhe/clifford-group-equivariant-neural-networks>

features of the network consist of mean-subtracted positions of the particles, the charge of each particle and their initial velocities. The edge attributes are the product of charges for connected node pairs. The goal of each model is to predict the displacement of each particle after 1000 timesteps. To ensure translational invariance, we subtract the mean positions from the particles’s positions. For all the baselines models, namely GNN [30], Tensor Field Network [66], SE(3)-Transformers [25], Radial Field [44], EGNN [58], SEGNN [12], and CGENN [57], we use the results reported by [57].

**Hyperparameter settings.** We maintain the set of hyperparamters similar to the set of hyperparamters specified in the source code of the original CGENN model. Especially, for CG-EGNN-1 and CG-EGNN-1-2, we set the learning rate to  $1 \times 10^{-3}$ , weight decay to  $1 \times 10^{-4}$ , hidden dimension to 20, and the number of layer to 3. We train the model with Adam optimizer and cosine anealing learning rate scheduler [47], batch size 100 for 100000 iterations, and we report the result on the test set at the point where the model checkpoint achieved the lowest MSE loss on the validation set.

*Appendix F.2. CMU Motion Capture with GMN settings.*

**Experimental settings.** In this experiment, we adapt the source code provided by [39]<sup>3</sup>. Specifically, we consider the walking motion of the human subject (subject #35) and adopt the random split used by [39, 33] with 495/498/498 splits for training/validation/testing. The node features of the network contains initial velocities and positions of each joint. We augment the set of original edges representing the joints of the human figure with 2-hops neighbors following [39, 33]. The edge feature contains two components: the first component takes value 2 if the edge is a two-hop edge and 1 otherwise, the second component takes value 1 when the edge is a stick and takes value 2 when the edge is a hinge, and takes value 0 otherwise. In this task, the prediction output corresponds to the location of each joint after 30 frames. For other baseline models, including: GNN [30], Tensor Field Network [66], SE(3)-Transformers [25], Radial Field [44], EGNN [58], GMN [39], we use the result reported from [39].

**Hyperparameter settings.** We keep the set of hyperparamters similar to the set of hyperparamters specified in the source code of the GMN [39] paper. For CG-EGNN-1 and CG-EGNN-1-2, we found we can the hidden dimension can be reduced to 16 without affecting the performance. We set the learning rate to  $5 \times 10^{-4}$ , weight decay to  $1 \times 10^{-10}$ , hidden dimension to 16, and the number of layers to 4. The model is trained with Adam optimizer for 500 epochs with batch size 100, and we report the performance of the model on the test set with the lowest validation loss.

---

<sup>3</sup><https://github.com/hanjq17/GMN>

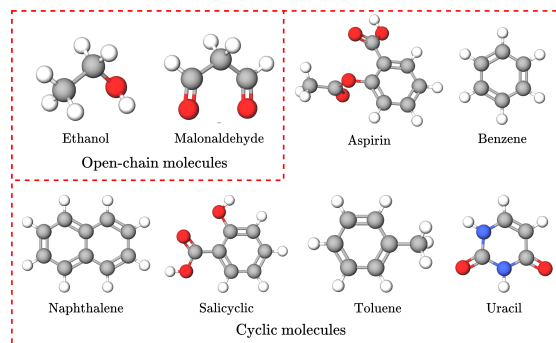


Figure F.2: Ball-and-stick model of molecules in MD17. Our method attains lower MSE for molecules with more complex structures.

### Appendix F.3. CMU Motion Capture with EGHN settings

**Experimental settings.** We use the source code adapted from EGHN paper [33]<sup>4</sup> for this experiment. Specifically, we use the same random split in [33]. The node features contains the velocities, positions and the augmented  $z$ -axis of each joint. The set of original edges are also augmented with 2-hops neighbors. The edge feature takes value 2 if the edge is a two-hop edge and 1 otherwise. In this task, the prediction output also corresponds to the location of each joint after 30 frames. Other baselines models in this experiment includes: GNN [30], Tensor Field Network [66], SE(3)-Transformers [25], Radial Field [44], EGNN [58], GMN [39], EGHN [33]. Asides from our model and CGENN, performance of other models follows from paper [33].

**Hyperparameter settings.** In this experiment, we keep the set of hyperparameters similar to the set of hyperparameters specified in the source code of the GMN [33] paper. Specifically, for CG-EGNN-1 and CG-EGNN-1-2, we also decrease the hidden dimension to 8, set the learning rate to  $5 \times 10^{-4}$ , weight decay to  $1 \times 10^{-12}$ , and fix the number of layers at 4. The model is trained using the Adam optimizer, using early-stopping of 50 epochs.

### Appendix F.4. MD17 experiment.

**Experimental settings.** In this experiment, we adopt the MD17 dataset [16], which consists of trajectories of eight different molecules generated through molecular dynamics simulation. We utilize the source code adapted from [39]<sup>5</sup> for this task and keep all settings the same. In which, we adopt the random split used by [39] to divide the dataset into 50% for training, 25% for validation, and 25% for testing. The time interval between the input and prediction frames is  $T = 5000$  timesteps. For this task, the feature node of each atom consists of

<sup>4</sup><https://github.com/hanjq17/EGHN>

<sup>5</sup><https://github.com/hanjq17/GMN>

the initial position, velocity and charges of the atom. The edge attribute is the concatenation of the atom number and its edge type indicator. The task of this experiment is to predict the future position of each atom given the current state of the molecule. We only consider the prediction for the position of large atoms and mask out all hydrogen atoms. Similar to [39], the graph of the molecule are also augmented with 2-hop neighbors. All the results of baseline models in this experiment are as reported from paper [39].

**Hyperparameter settings.** In this experiment, we use the same hyperparameter setting for both CG-EGNN-1 and CG-EGNN-1-2 for all molecule tasks. In which, we set the learning rate to  $5 \times 10^{-4}$ , weight decay to  $1 \times 10^{-10}$ , reduce the hidden dimension to 8, and set the number of layers to 4. The models are trained with Adam optimizer for 500 epochs with batch size 100 and report the result on the test set at the checkpoint with the lowest MSE loss on the validation set.

#### *Appendix F.5. 5D Convex Hulls*

**Experimental settings.** In this experiment, we utilize the source code provided by [57] and [46]<sup>6</sup> for the Convex Hulls experiment. The implementation of CGENN is adapted from [57], the implementation of CSMPN [46] is adapted from [46]. Specifically, we generate a dataset of 16384 convex hulls with 8 vertices samples for each of the train, validation, and test set. Each convex hull is constructed by randomly sampling eight points from a standard normal distribution. To ensure a fair comparison, we keep the number of parameters in our implementations similar to [46] and maintain the same experimental settings. We compare our models with the following baselines: GNN [30], EGNN [58], CGENN [57], EMPSN [22], and CSMPN [46].

**Hyperparameter settings.** In this experiment, we keep the set of hyperparameters similar to the set of hyperparameters specified in the source code of [46] paper. Specifically, for CG-EGNN-1 and CG-EGNN-1-2, we also decrease the hidden dimension to 16, set the learning rate to  $1 \times 10^{-3}$ , and fix the number of layers at 4. The model is trained using the Adam optimizer, using early-stopping of  $1 \times 10^5$  iterations.

#### *Appendix F.6. Ablation study on the effect of including high order messages on 3D convex hull dataset*

**Experimental settings.** For this experiment, we create 3 dataset of 3D convex hulls with number of nodes per graph  $\in \{6, 7, 8\}$ . Each vertice is sampled from a standard normal distribution to obtain 3 dataset of 4000/4000/4000 samples for training/validation/test each. We run all 3 dataset for baselines GNN [30], EGNN [58], CGENN [57], and CG-EGNN models with all possible combination of message orders up to message order 3 (namely, the following list of combinations:  $\{1, 2, 3, 1-2, 1-3, 2-3, 1-2-3\}$ ).

---

<sup>6</sup><https://github.com/congliuUvA/Clifford-Group-Equivariant-Simplicial-Message-Passing-Networks>



Table F.5: MSE ( $\times 10^{-2}$ ) of the 3D Convex Hulls experiment. The best CG-EGNN message orders combinations with 1, 2, 3 elements are highlighted. The best model for all combination of message orders is CG-EGNN-1-2-3.

| Nodes<br>in graphs | GNN   | EGNN  | CGENN | CG-EGNN message orders |               |       |               |        |        |               |
|--------------------|-------|-------|-------|------------------------|---------------|-------|---------------|--------|--------|---------------|
|                    |       |       |       | 1                      | 2             | 3     | 1-2           | 1-3    | 2-3    | 1-2-3         |
| 6                  | 6.472 | 7.347 | 6.251 | 2.531                  | <b>0.8410</b> | 1.057 | <b>0.5604</b> | 0.5683 | 0.7838 | <b>0.3970</b> |
| 7                  | 12.60 | 10.85 | 25.48 | 4.690                  | <b>2.379</b>  | 2.865 | <b>1.665</b>  | 2.080  | 1.809  | <b>1.064</b>  |
| 8                  | 24.45 | 12.05 | 55.47 | 9.487                  | <b>4.782</b>  | 6.934 | <b>4.042</b>  | 4.731  | 5.899  | <b>3.660</b>  |

Table F.6: Runtime (second/it) of the 3D Convex Hulls experiment.

| Nodes<br>in graphs | GNN      | EGNN     | CGENN   | CG-EGNN message orders |        |        |        |        |        |        |
|--------------------|----------|----------|---------|------------------------|--------|--------|--------|--------|--------|--------|
|                    |          |          |         | 1                      | 2      | 3      | 1-2    | 1-3    | 2-3    | 1-2-3  |
| 6                  | 0.005421 | 0.005735 | 0.01792 | 0.1159                 | 0.1256 | 0.1270 | 0.1817 | 0.1838 | 0.1948 | 0.2554 |
| 7                  | 0.005512 | 0.005831 | 0.01826 | 0.1170                 | 0.1496 | 0.1739 | 0.2140 | 0.2394 | 0.2722 | 0.3365 |
| 8                  | 0.005785 | 0.006169 | 0.01923 | 0.1234                 | 0.1962 | 0.2944 | 0.2669 | 0.3664 | 0.4374 | 0.5124 |

**Hyperparameter settings.** We set the hidden dimensions of GNN, EGNN, CGENN to 32 and hidden dimensions of CG-EGNN models of all order combinations to 8. The learning rate is set to  $1 \times 10^{-3}$ , number of layers is 4, all models are trained using Adam optimizer with early-stopping for  $5 \times 10^4$  iterations.

## Appendix G. Broader Impact

The introduction of Clifford Group Equivariant Graph Neural Networks (CG-EGNNs) in this paper holds significant societal impact by advancing the capabilities of neural networks to handle data symmetry, particularly in applications requiring precise geometric representations. This innovation has the potential to drive progress in fields such as drug discovery, materials science, and robotics, where accurate modeling of molecular and physical systems is essential. By enhancing the expressive power and maintaining equivariance properties, CG-EGNNs can lead to more accurate simulations and predictions, reducing the time and cost associated with experimental procedures. Furthermore, the improved performance on benchmarks like n-body simulations, CMU motion capture, and MD17 showcases the practical utility of CG-EGNNs in real-world scenarios. As these advanced neural networks become more integrated into scientific research and industry, they could facilitate breakthroughs in developing new materials, understanding complex biological processes, and creating sophisticated autonomous systems, ultimately contributing to technological advancements and improving quality of life.